Indian Geotechnical Journal, 39(1), 2009, 1-63

Numerical Analysis of Underground Structures*

K.G. Sharma**

Introduction

A large number of river valley projects, metro rail, underground oil/gas storage and nuclear repository projects are under planning and construction in the country. Underground structures form the integral part of these projects. The vital feature of the analysis and design of these structures is the characterization of behaviour of roc_ks and rock masses. The design of underground structures essentially consists of designing the cross-section and support systems consistent with the functional requirement and the characteristics of the rock formation. The design methods include empirical methods based on experience, closed form solutions that use simplifying assumptions and numerical methods. With the phenomenal growth in the development of computers and softwares, powerful and versatile numerical methods are increasingly adopted in the analysis and design of underground structures. Among the numerical methods, finite element, boundary element and distinct element methods are commonly used. These methods facilitate modelling of a wide range of behaviour related to rock mass and support system. The attractive feature of these methods is that practically any complex behaviour including elastic, elasto-plastic and strain softening behaviour exhibited by materials can be easily incorporated. Another distinguishing feature of these methods is that various sequences of excavation and installation of support system can be simulated. In this paper, the physical and material characterizations of rock are discussed. Various numerical modelling techniques used for the study of underground structures are briefly presented. The applications of the numerical methods for the analysis of various underground structures are dealt with in detail in the paper.

The contents of the presentation are primarily those with which the author has been associated with over the last 25 years.

Underground Structures in India

Many underground structures have been constructed in India during the last few decades particularly for hydropower and irrigation projects in a wide variety of geological settings ranging from the fragile Himalayas to relatively stable peninsular region. Tunnels have also been built for water supply, sewage

---

* Annual Lecture, Indian Geotechnical Conference IGC 2008, Bangalore, 17 Dec '08

** Professor, Department of Civil Engineering, Indian Institute of Technology Delhi, Hauz Khas, New Delhi – 110016, India. Email: kgsharma@civil.iitd.ernet.in

disposal, highways, railways, and metros. Many more underground structures are in the planning and construction stage to meet the ever-growing demands for irrigation, hydropower, drinking water, transportation, oil and gas storage, and nuclear waste storage.

New hydropower projects are being taken up involving construction of more than 1000 km length of tunnels with sizes varying from 2.5 to 14 m diameter to add 16500 MW of hydropower by the end of 11th Five year plan. After the success of metro rail project in Delhi with the state-of-the-art technology, the construction of metro rail project is planned in various cities including Mumbai, Bangalore, Hyderabad, Lucknow, Pune, and Chandigarh. The Indian Railways is constructing the most challenging Jammu-Udhampur-Srinagar-Baramulla railway line in the difficult Himalayan terrain of Jammu and Kashmir and there are 42 tunnels of total length 107.96 km in the Katra-Quazigund section (142 km). The Konkan Railway Corporation has constructed 760 km Konkan railway line with 92 tunnels of total length 83.6 km. The Border Roads Organisation has planned a prestigious and challenging highway tunnel with a length of 8.9 km under the 3978 m high Rohtang pass on Manali-Leh road and the construction of the tunnel is to start shortly.

Among the existing tunnels, nearly 70% of them are used for hydropower projects. The shapes used are predominantly D-type, horse-shoe and circular. Conventional drilling and blasting method remains practically the dominant practice for tunnel excavation in India. Attempts have been made in the past to use tunnel boring machines (TBMs) with success in some and failure in others. For Delhi metro, TBMs and EPBMs have been used successfully.

Until recently, barring a few cases, the use of steel ribs with backfilling by tunnel muck or lean concrete was practically the only method of supporting in India. Lately there has been a considerable increase in the use of shotcrete as a support system particularly for large underground cavities. The use of steel fibre reinforced shotcrete (SFRS) has also been made in few projects such as Uri Project (Jammu and Kashmir), Nathpa-Jhakri Project (Himachal Pradesh), Srisailam Project (Andhra Pradesh) and Koyna Project (Maharashtra). SFRS is being used increasingly now.

Rock Characterisation

Rock, unlike other engineering materials, may include joints and joint sets. The scale of the geometry of the engineering structure and the frequency of joints are the factors which are to be considered in physical characterization of the rock (Hoek, 1983; Brady, 1987). Brady (1987) categorized the rock mass in four basic physical models (Figure 1); a) continuum, b) continuum with a few predominant joints, c) rock with well defined joint sets, and d) frequently and randomly fractured rock mass which may be considered as pseudo-continuum.

Rock as a continuum may exhibit elastic, elasto-plastic or brittle behaviour depending upon the type of rock and the stress imposed by an engineering structure. The joints/discontinuities are the main sources of weakness for the rock. The nature and the condition of the joints may vary widely from the freshly broken rough surfaces to smooth slickenside surfaces consisting of the joints filled with soft gouge material. The characterization of

the joint behaviour may range from simple elastic behaviour based on relative movements to complicated elasto-plastic behaviour. The behaviour of rock with well defined joints sets is rather difficult to characterize using classical theories. Various attempts have been made ranging from modification of classical theories to include the effect of joint sets to equivalent material model.

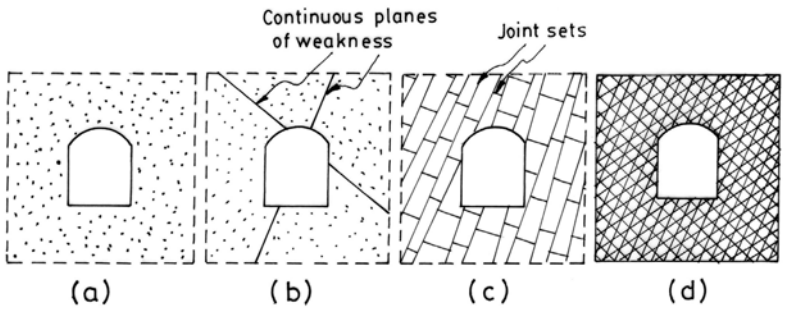

Fig. 1 Conceptual Models Relating Rock Structures to Excavation (Brady, 1987)

Numerical Methods

The analytical solutions are available for deep tunnels having circular, elliptical, rectangular with rounded corners, ovaloid, spheriodal shapes and for circular opening at shallow level considering rock to be homogeneous, elastic and isotropic (Obert and Duvall, 1967; Poulos and Davis, 1974; Terzaghi and Richart, 1952) and for deep circular and spherical tunnels excavated in rock medium having isotropic in-situ stresses for von-Mises, Mohr-Coulomb, Hoek-Brown yield criteria (Obert and Duvall, 1967; Goodman, 1989; Hoek and Brown, 1980). Special and complex structures such as intersections, bifurcations, stacked tunnels and interaction of several tunnels in closed proximity and openings of complex shapes excavated in rock medium with complicated properties can not be analysed by simple analytical solutions. Stress-deformation analysis and the requirement of supports in such cases can be analysed only by numerical methods.

Two approaches to numerical modeling of rock masses can be identified, both recognizing geological structures as being discontinuous due to joints, faults and bedding planes. A continuum approach treats the rock mass as a continuum intersected by a number of discontinuities, while a discontinuum approach views the rock mass as an assemblage of independent blocks or particles.

The finite difference method (FDM), finite element method (FEM) and boundary element method (BEM) are based upon the continuum approach. The FEM involves eight basic steps viz., discretisation, selection of displacement model, definition of strain-displacement and stress-strain relations, derivation of element equations, assembly and incorporation of boundary conditions, solutions of primary unknowns, computation of secondary unknowns, and interpretation of results. These steps are described in detail in various books on FEM (e.g. Desai and Abel, 1972; Zienkiewicz and Taylor, 1989; Bathe, 1982). The FEM can be used to analyse problems with material and geometric nonlinearities, complex boundary conditions and non-homogeneities. The method involves discretisation of the entire region of interest.

Boundary element method (BEM) involves the discretisation of the interior or exterior boundaries only and consists basically of definition and solution of a problem entirely in terms of surface values of traction and displacement (Banerjee and Butterfield, 1981; Crouch and Starfield, 1983; Brady, 1987). BEM is classified as direct and indirect depending on the procedure used to construct relationships between the tractions and the displacements. Indirect formulation is used in rock engineering problems particularly with respect to underground structures.

Discontinuum models feature numerical procedures involving the equations of blocks or particles rather than continuum. Cundall (1971) was among the first to implement the distinct element method (DEM) to represent rock mass as an assembly of discrete blocks where joints/discontinuities are viewed as interfaces between distinct bodies. This method is based on an explicit time stepping algorithm for the integration of the equations of motion of the system in the time domain. The scheme allows for an efficient treatment of the nonlinear phenomena such as sliding, separation and large deformations occurring in the mathematical model.

Simulation of Excavation

The simulation of the method of excavation consists of a series of steps (stages), each step representing the removal of one lift of the stressed material from a continuous body. The procedure for one-step excavation is illustrated in Figure 2.

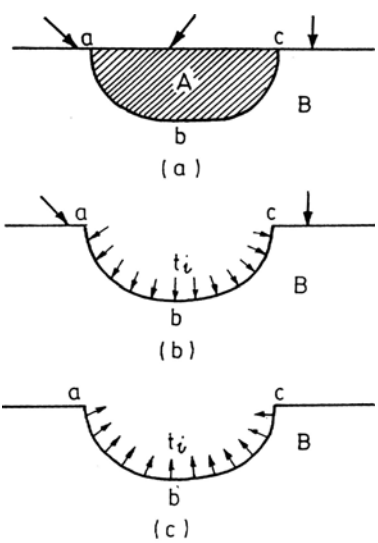

Fig. 2 The Excavation Procedure

Figure 2(a) shows an initial stressed body of soil or rock from which the shaded portion A is to be excavated. The remaining portion is labelled as B. The traction, t_i, exerted by region A on region B in the initially stressed body is shown

in Figure 2(b). Now the excavation process involves removing the elements and stiffness of portion A and traction, t_i from the portion B in Figure 2(b). This is done by applying to the portion B traction $-t_i$ (equal and opposite to t_i) as shown in Figure 2(c). This results in the stress free excavation surface abc. Using the stiffness of portion B and traction $-t_i$, incremental displacements, strains and stresses are obtained and these are added to the original values for the portion B.

Sharma et al. (2001) presented a finite element formulation along with detailed algorithm for simulating multi-stage excavation in elasto-plastic geologic medium. The excavated elements and nodes are eliminated during assembly in this algorithm, thus it is not necessary to use "air" elements, static condensation and matrix partitioning as it was done in previous processes by others (Sharma et al., 1985b; Chandrasekaran and King, 1974; Borja et al., 1989; Ghaboussi and Pecknold, 1984; Comodromos et al., 1993). Due to this, the algorithm is very efficient and accurate. The proposed algorithm was implemented in computer program DSC-SST-2D (Desai, 1997) developed for 4-noded and 8-noded solid elements in FORTRAN-90 language using the elasto-plastic finite element procedure given in Desai et al. (1991).

Analysis by Finite Element Method

In this section, analysis of typical tunnels and underground powerhouse caverns using FEM along with important conclusions drawn is presented.

Elasto-Plastic Analysis of Circular and Horse-Shoe Tunnels

Srivastava (1985), Sharma et al. (1985b) and Srivastava et al. (1986a & b, 1987) carried out two-dimensional elastic and elasto-plastic finite element analyses of circular and horse-shoe tunnels for different values of insitu stress ratio (K_o = 0.5, 1.0 and 1.5). Hoek-Brown yield criterion was used for the elasto-plastic analysis. Here the typical results are presented for horse-shoe tunnel.

Elastic and elasto-plastic finite element analyses have been conducted on horse-shoe shaped tunnel with width and height equal to 8m located at a depth of 250 m for single and two stage excavations under three stress ratio (K_o) values of 0.5, 1.0 and 1.5 (Srivastava et al., 1987). The rock is of good quality Basalt and the material properties used for the analysis are given in Table 1.

Table 1 Properties of Basalt

Properties	Value
Young's modulus, E	3.5×10^4 MPa
Poisson's ratio, ν	0.21
Unconfined compressive strength, σ_c	122.364 MPa
Tensile strength, σ_t	0.2447 MPa
Vertical insitu stress, σ_{v0}	6.75 MPa
Hoek-Brown strength parameter m	1.70
Hoek-Brown strength parameter s	0.004

The displaced shape of the tunnel for various cases for K_o = 0.5 are shown in Figure 3. For single stage excavation, elasto-plastic analysis showed higher displacements in the side wall. For two stage excavation, the displacement pattern predicted by the elasto-plastic analysis is different from that predicted from single stage excavation. The displacement paths for single and two stage excavations are presented at various points in Figure 4. It is shown that the excavation sequence has significant effect on the displacements.

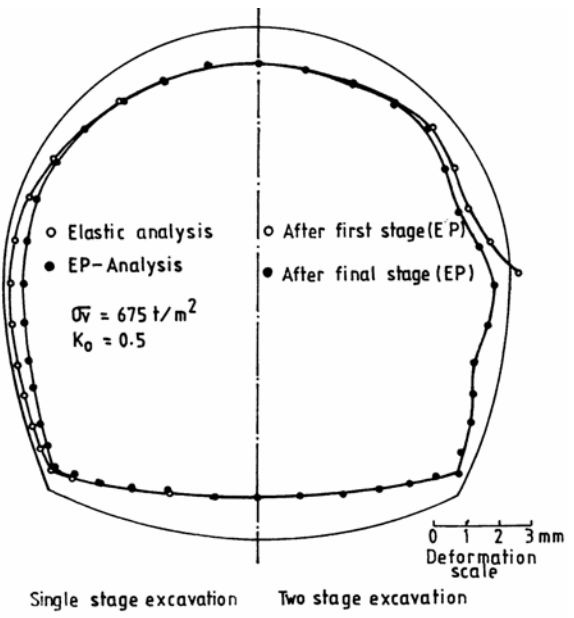

Fig. 3 Deformed Shape of Tunnel

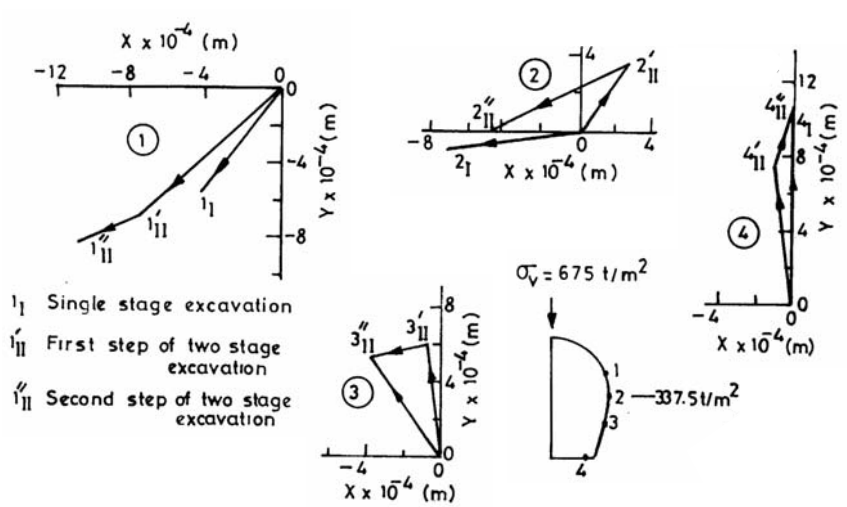

Fig. 4 Displacement Paths for Elasto-plastic Analysis

Comparison of displacements and stresses at typical locations are presented in Table 2 for various cases studied. The important finding of these studies is that the sequence of excavation can result in large reversal of stresses and in the direction of movement of the points around the tunnel.

From the analysis, it was concluded that circular shape appears to be better for $K_o \geq 1$ and horse-shoe shape for $K_o < 1$.

Table 2 Stresses and Displacements near Tunnel Boundary (K_o = 0.5)

	Location	Single stage excavation			Two stage excavation	
		EL	EP	Percentage difference between EP and EL	EP	Percentage diff. between two stage & single stage excavation
Resultant Displacement x 10^{-3} m	1	0.515	0.704	36.76	1.289	83.07
	2	0.280	0.649	131.99	3.471	-27.51
	3	0.491	0.634	29.09	0.661	4.21
	4	0.994	1.013	1.94	1.020	0.70
Minor principal stress (kPa)	1	274.0	269.0	1.75	392.0	45.50
	2	1.0	129.0	Large	16.7	-86.90
	3	30.0	-1.0	104.4	8.1	703.50
Major principal stress (kPa)	1	12858.0	11162.0	15.19	7716.0	-30.87
	2	12676.0	9362.0	35.39	8162.0	-12.81
	3	7203.0	7126.7	1.06	7124.3	-0.03

EL – elastic analysis Locations 1, 2, 3 and 4 as per Figure 4.

EP – elasto plastic analysis

Sharma and Sharma (1986) used finite element method to analyse circular and D-type tunnels in isotropic and transversely isotropic rock medium for different insitu stress conditions (K_o = 0.5, 1.0, 1.5). Plane strain case has been considered. Effect of anisotropy was clearly depicted in deformed shapes of the openings. The zone of influence of principal stresses was affected by the anisotropy but the effect was not that significant as in the case of deformations.

Elasto-Plastic Analysis of Interacting Tunnels

Srivastava (1985), Sharma et al. (1985c) and Srivastava et al. (1988, 1989) carried out elastic and elasto-plastic analyses of two circular interacting tunnels of 8 m diameter located at a depth of 250 m from the ground surface. Three pillar width/tunnel diameter (W/D) ratios of 0.3, 0.6 and 1.2 have been chosen and three in-situ stress ratios (K_o = 0.5, 1.0 and 1.5) have been considered. The material properties of Table 1 are used in the analyses. The tunnels are considered to be excavated simultaneously and sequentially. In case of simultaneous excavation, both tunnels are excavated (full face) in a single stage whereas in the case of sequential excavation, first right hand side tunnel is excavated (full face) and then in next stage, the left hand side tunnel is excavated (full face). In the present paper, typical results for W/D = 0.3 are presented.

Figure 5 shows schematically the various cases analysed. The yield zone and deformed shapes of the tunnels for K_o = 0.5 and 1.5 are shown in Figures 6 and 7, respectively. It has been found that the yielded zone is highest for K_o = 1.5 and smallest for K_o = 0.5. For K_o = 1.0, the yielded zone falls in between.

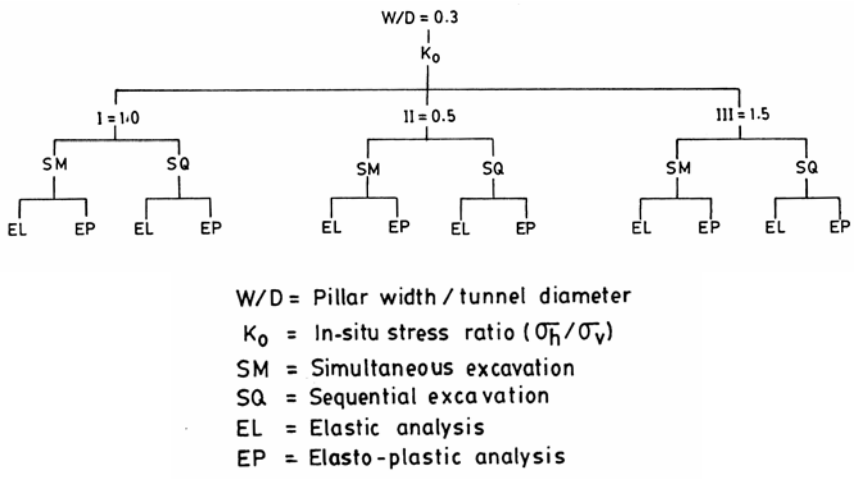

Fig. 5 Schematic Diagram – Various Cases Analysed for Interacting Tunnels

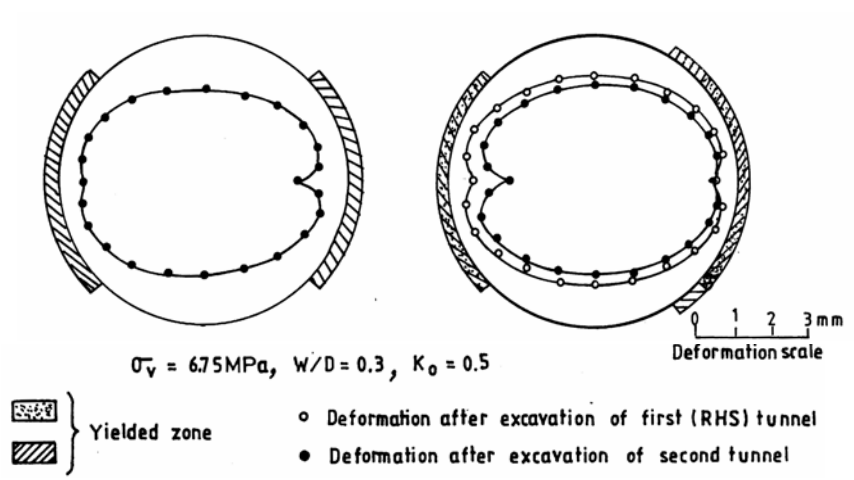

Fig. 6 Deformed Shape of Interacting Tunnels and Yielded Zones- Sequential Excavation, EP Analysis, K_o = 0.5

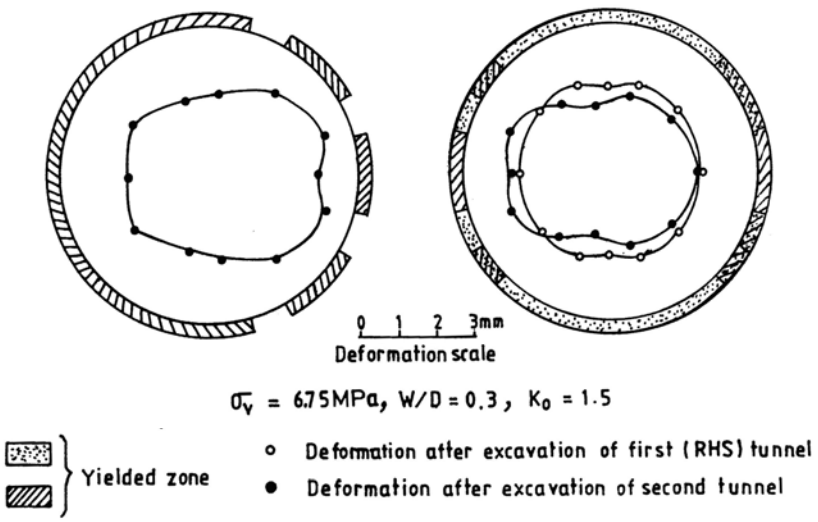

Fig. 7 Deformed Shape of Interacting Tunnels and Yielded Zones- Sequential Excavation, EP Analysis, K_o = 1.5

Table 3 shows the displacements at three typical locations (crown and springing levels on the abutment and pillar sides) for various cases. It is observed that the deformations at tunnel boundary at springing level on pillar side are least for elastic case and maximum for elasto-plastic case. The difference between elastic and elasto-plastic analyses is reflected more in the case of smaller insitu stress ratio of K_o = 0.5.

Table 3 Displacements (mm) at the Boundary of Interacting Tunnels (W/D = 0.30)

Location	K_o = 1.0			K_o = 0.5			K_o = 1.5		
	SMEL	SMEP	SQEP	SMEL	SMEP	SQEP	SMEL	SMEP	SQEP
1	0.91	1.24	1.26	0.18	0.78	0.83	1.65	1.73	1.72
2	1.22	1.26	1.44	1.37	1.42	1.42	1.09	1.85	2.30
3	0.27	1.48	1.57	0.17	1.61	1.76	0.38	1.39	1.43
1’	0.91	1.24	1.24	0.18	0.78	0.78	1.65	1.73	1.79
2’	1.22	1.26	1.26	1.37	1.42	1.42	1.09	1.85	1.85
3’	0.27	1.48	1.46	0.17	1.61	1.61	0.38	1.39	1.32

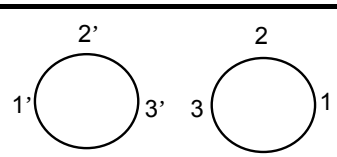

EL - elastic analysis
EP - elasto-plastic analysis
SM - interacting tunnels, simultaneously excavated
SQ - interacting tunnels, sequentially excavated

Elastic Analysis of a Powerhouse Cavern in Gujarat

As a part of Sardar Sarovar hydropower project constructed across Narmada river in Gujarat State in western part of India, an underground powerhouse cavern is constructed on the right abutment with the capacity of 1200 MW. The powerhouse is D-shaped with 23 m width and 57.6 m height and is located at a distance of 67.5 m from the toe of the dam (Figure 8). The crown of the cavern is about 45 m below the ground surface. The powerhouse cavern is located in basalt rock. At this section, two shear zones exist as shown in the Figure 8. The shear zones are filled with weathered material similar to sand and their thickness varies from 2 m to 5 m.

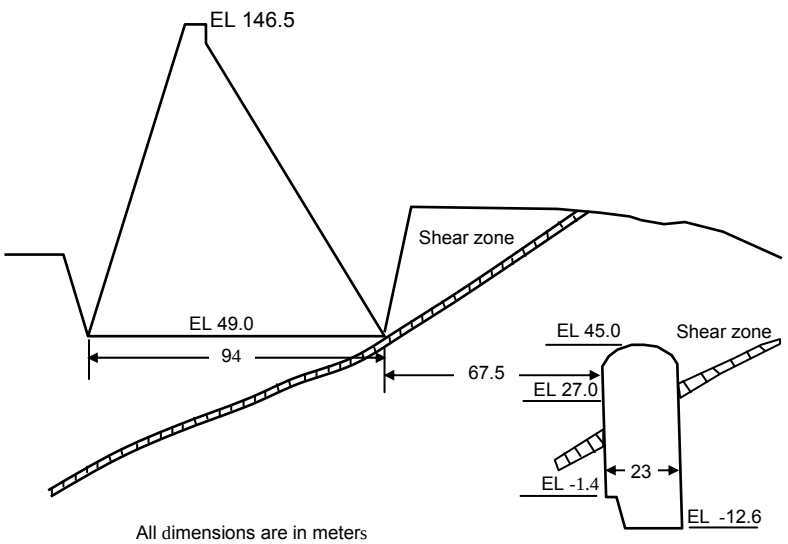

Fig. 8 Details of Powerhouse Cavern

To investigate the behaviour of the cavern as affected by the loading due to excavation and reservoir loading, Varadarajan and Sharma (1984a) carried out two-dimensional elastic finite element analysis. The finite element mesh used for the analysis along with boundary conditions is shown in Figure 9. A total of 407, eight-noded isoparametric elements with 1288 nodes were used for discretisation. Plane strain condition was assumed to prevail.

The material properties for the rock and shear zone are:

	Rock	**Shear zone**
Young's modulus	5.5×10^7 kPa	1.0×10^7 kPa
Poisson's ratio	0.21	0.25
Unit weight	26.5 kN/m^3	26.5 kN/m^3
In-situ stress ratio	0.65	0.65

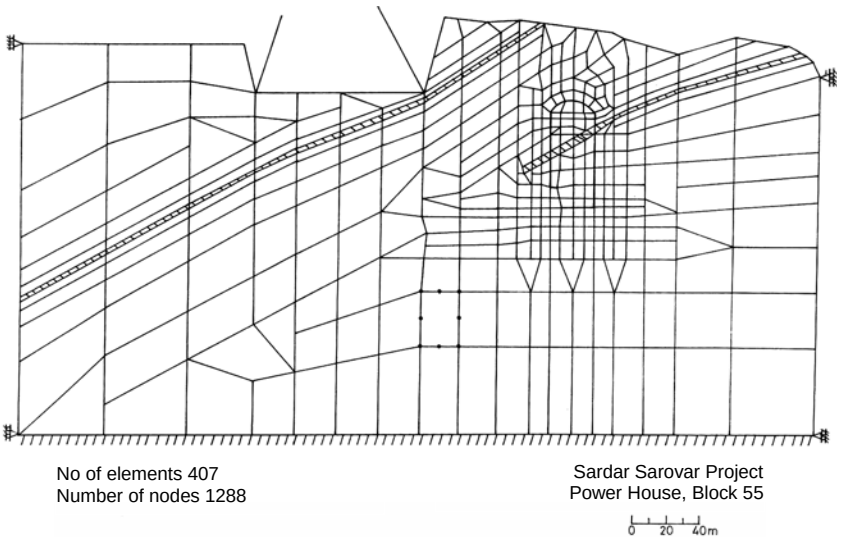

Fig. 9 Finite Element Discretization of Powerhouse Cavern

The dam loading (from separate analysis) when the reservoir is full is shown in Figure 10 and is applied at the base of the dam and on the grout curtain. The analysis was conducted with excavation and dam loadings. The displacements and the stresses were calculated from the analysis. The induced stresses were superimposed on the in-situ stresses to get the resultant values of the stresses.

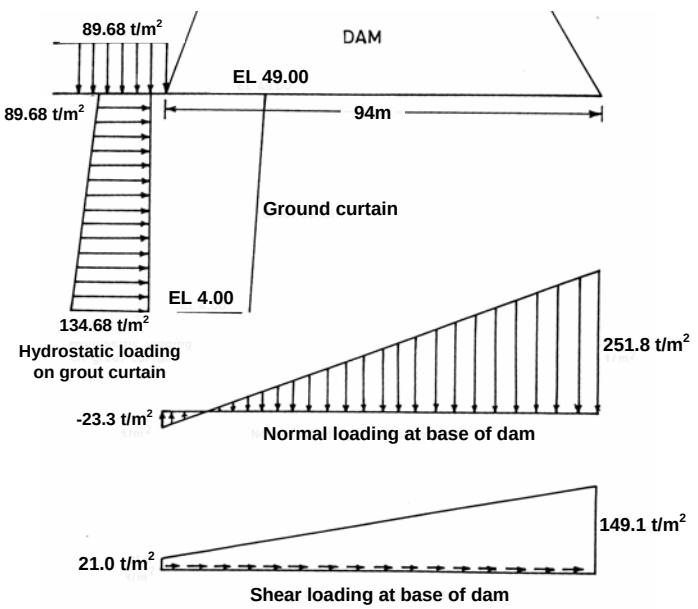

(1 t/m^2 = 10 kPa)

Sardar Sarover Project, Power House

Fig. 10 Loading due to Reservoir

The displaced shapes of the cavern due to excavation of the cavern and due to dam loading are shown in Figure 11. It may be noted that the movement of the left wall is slightly more than the right wall due to the excavation of the cavern and this may be due to unequal overburden. The dam loading causes rightward movement of the cavern and the increase in the wall movement on the left wall (14.5 mm to 30.0 mm) is significant as compared to the right wall (9.2 mm to 4.3 mm) movement. The vertical and horizontal displacement contours are shown in Figures 12 and 13. The contours of major and minor principal stresses are shown in Figures 14 and 15. It may be observed that the contours of stresses due to cavern excavation loading are unsymmetric with respect to the cavern. This may be due to the unequal overburden pressure and the presence of shear seams. It may also be noted that there is marked change in the nature of distribution and the magnitude of the displacements and stresses on the left side of the cavern due to the reservoir loading as compared to the right side of the cavern.

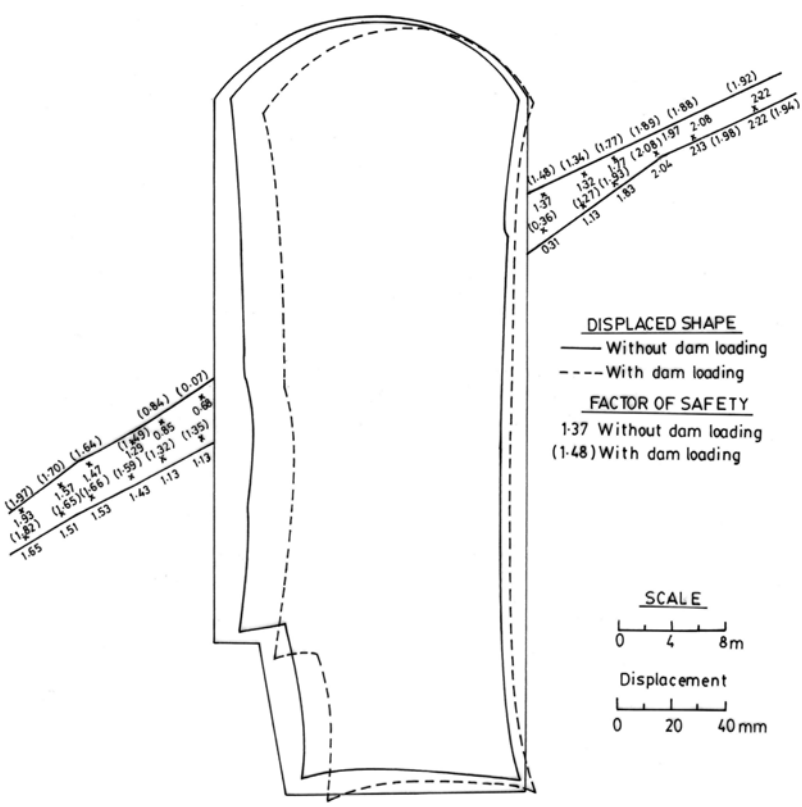

Fig. 11 Deformed Shape of Powerhouse Cavern

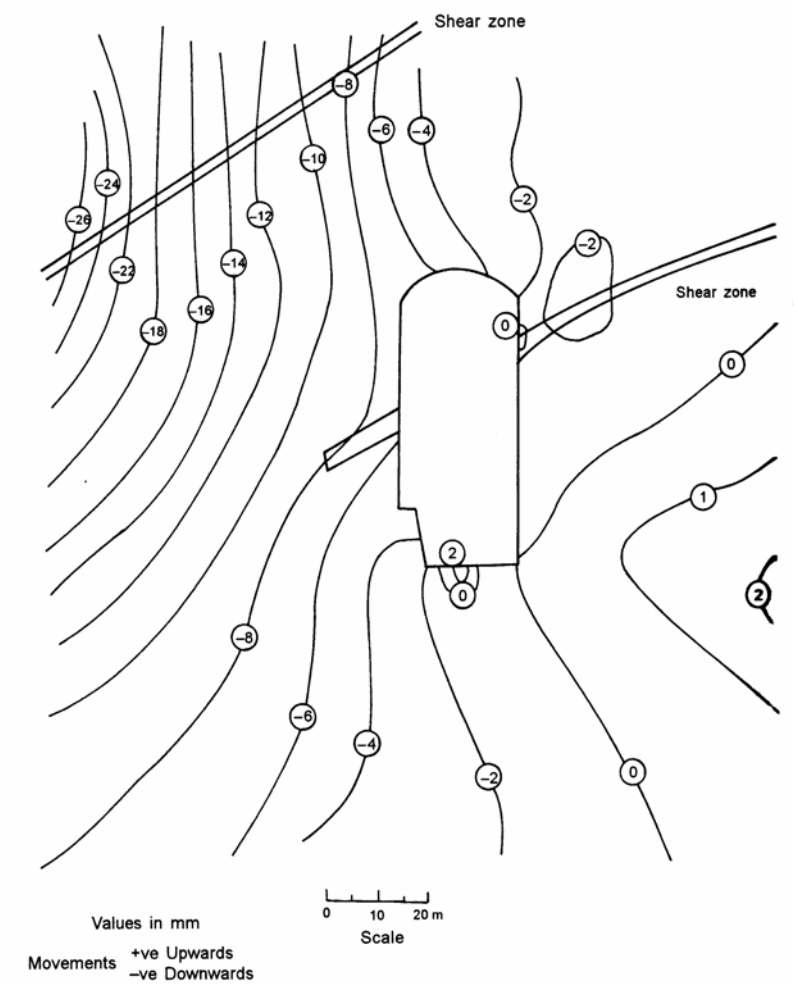

Fig. 12 Vertical Displacement Contours around the Cavern

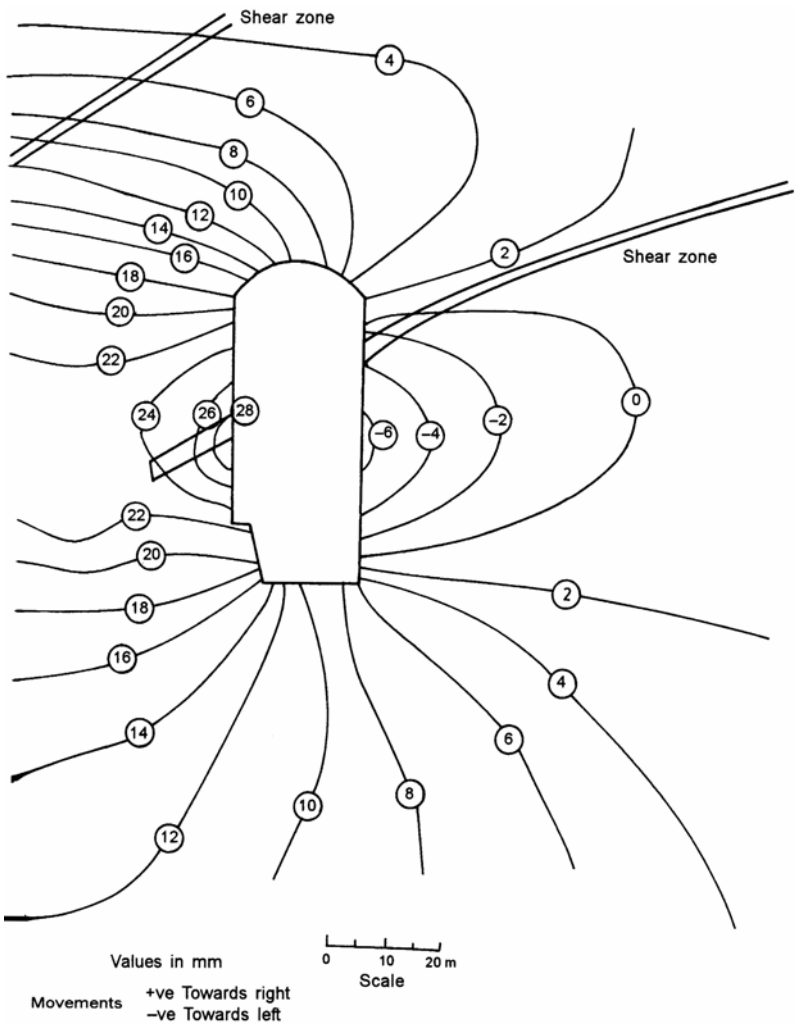

Fig. 13 Horizontal Displacement Contours around the Cavern

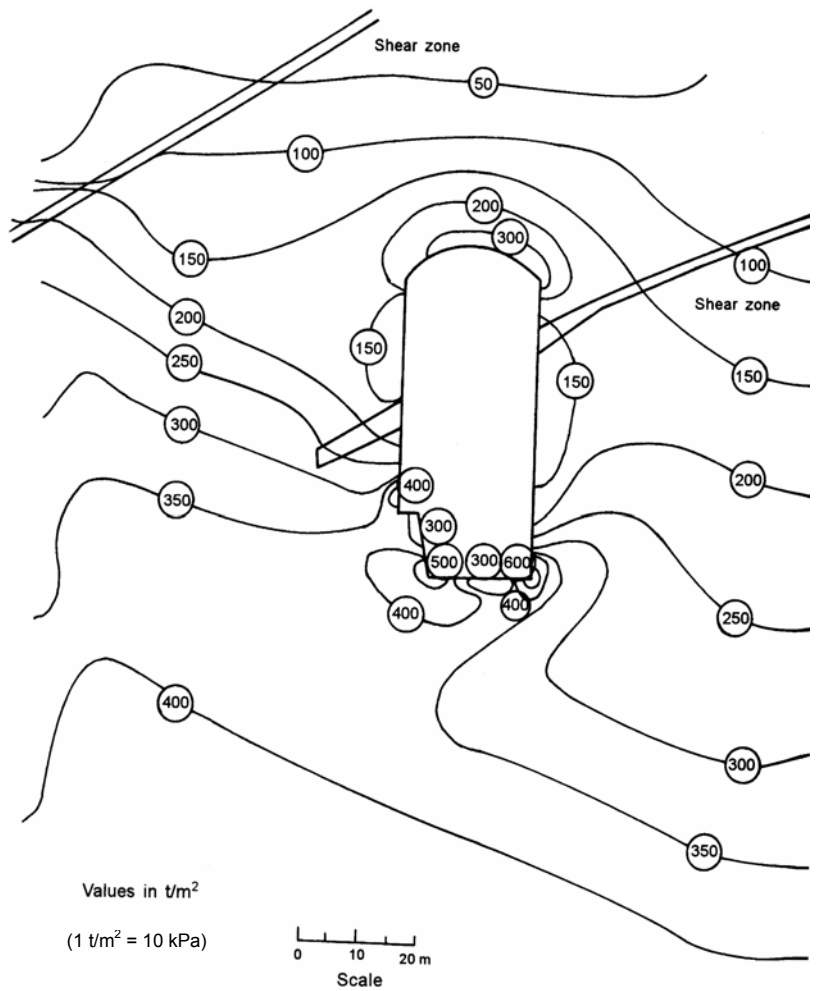

Fig. 14 Major Principal Stress Contours around the Cavern

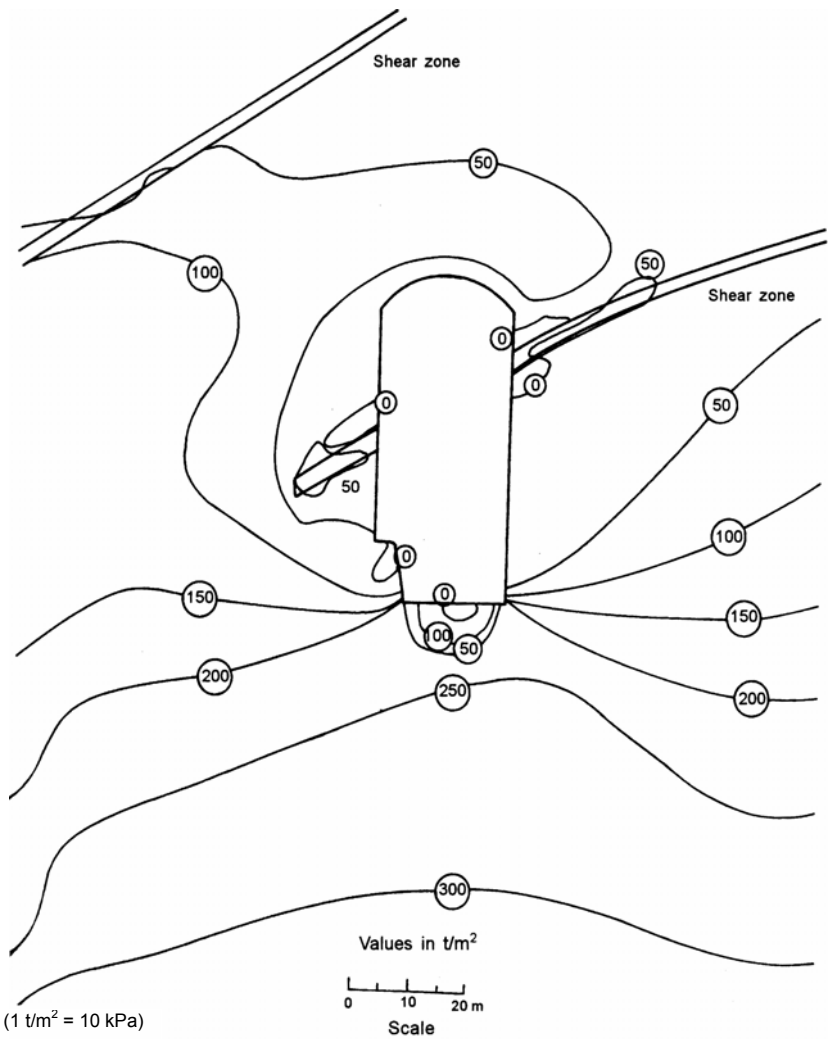

Fig. 15 Minor Principal Stress Contours around the Cavern

Elasto-Plastic Analysis of a Powerhouse Cavern in the Himalayas

The Nathpa-Jhakri Hydropower Project with an installed capacity of 1500 MW is constructed in the middle reaches of the river Satluj in Himachal Pradesh state in the northern part of the Indian subcontinent. The powerhouse complex of the project consists of two major openings, i.e., the machine hall 216 m x 20 m x 49 m (length x width x height) with an overburden of 262.5 m at crown and the transformer hall 198 m x 18 m which is located downstream of machine hall (Figure 16). The longitudinal axis of the openings is in the N-S direction. Based on the in-situ stress tests using hydraulic fracturing technique by the Central Soil and Materials Research Station (CSMRS), New Delhi, the vertical in-situ stress was found to be 5.89 MPa and the in-situ stress ratio worked out to be 0.8035.

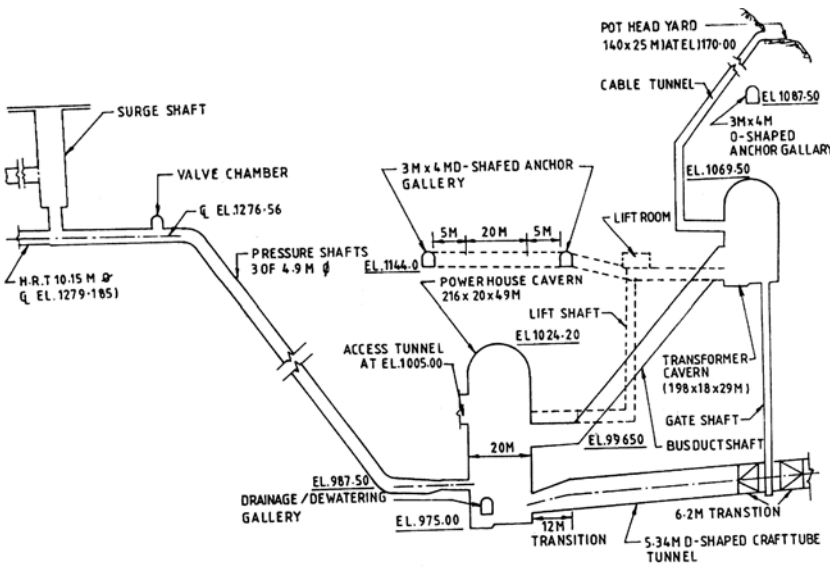

Fig. 16 East-west Section of Surge Shaft, Pressure Shaft and Powerhouse Cavern

Quartz mica samples were collected from the project site for testing. Strain controlled triaxial tests were conducted on the intact rock specimens using servo- controlled loading system at IIT Delhi (Hashemi, 1999). The constitutive model based on disturbed state concept (DSC) was used to characterize the behavior of the intact rock (Desai, 1994 & 2001). In this approach, the material response is expressed in terms of the responses in the continuous (relatively intact, RI) and discontinuous (fully adjusted, FA) parts through the coupling (disturbance) function. The relatively intact state is assumed as associated elasto-plastic hardening response and is characterised by Hierarchical Single Surface (HISS) model, (δ_0). Material parameters for the model were determined for the rock samples (i.e. intact rock) as indicated in Hashemi (1999) and Varadarajan et al. (2001a).

The material parameters for the rock mass have to be determined to carry out the finite element analysis of the powerhouse cavern. The procedure proposed by Ramamurthy (1993, 2001) to determine the strength and the Young's modulus of the jointed rock mass from the intact rock properties was

suitably adopted to determine the material parameters for the constitutive model. The parameters for the intact rock and rock mass are given in Table 4. The unit weight of the rock mass is taken as 27 kN/m^3.

Table 4 Material Parameters for Intact and Jointed Rock Mass

Type	Elasticity		Ultimate		Phase Change	Hardening		Bonding Stress (MPa)	Disturbance		
	ν	E (MPa)	γ	β	n	a_1	η_1	3R	D_u	A	Z
Intact Rock	0.20	8591	0.02020	0.46780	5.0	$13x10^{-15}$	0.6	46.99	0.97	220.7	1.339
Rock Mass	0.20	6677	0.01352	0.01352	5.0	$13x10^{-15}$	0.6	41.90	0.97	220.7	1.339

Hashemi (1999) and Varadarajan et al. (2001b) carried out finite element analysis of powerhouse cavern using computer code DSC-SST-2D developed by Desai (1997) using the constitutive model based on DSC. The effect of the excavation of the transformer hall on the powerhouse cavern (machine hall) is found to be negligible (Sharma and Bagde, 1994), and therefore only the excavation of the powerhouse cavern is considered. Twelve stages of excavation are used in the study as shown in Figure 17. In the analysis, the load due to each of the first nine stages is applied in single increment, whereas the load for each of the remaining stages is applied in three equal increments.

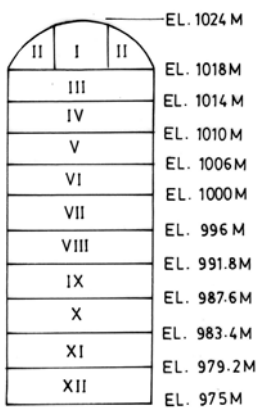

Fig. 17 Excavation Sequence for the Powerhouse Cavern

Since the loading and the geometry of the cavern are symmetric, only half of the portion is discretised. The cavern and the rock mass included for the discretisation are shown in Figure 18. The rock mass is discretised into 364 eight-noded isoparametric elements and 1167 nodes keeping in view various stages of excavation of the cavern. The in-situ vertical stresses are calculated from the ground at 262.5 m from the crown and the K_o value of 0.8035 as found from the tests has been used.

The results of the analysis are plotted as the contours of displacements, and principal stresses for the full excavation of the cavern at 12th stage.

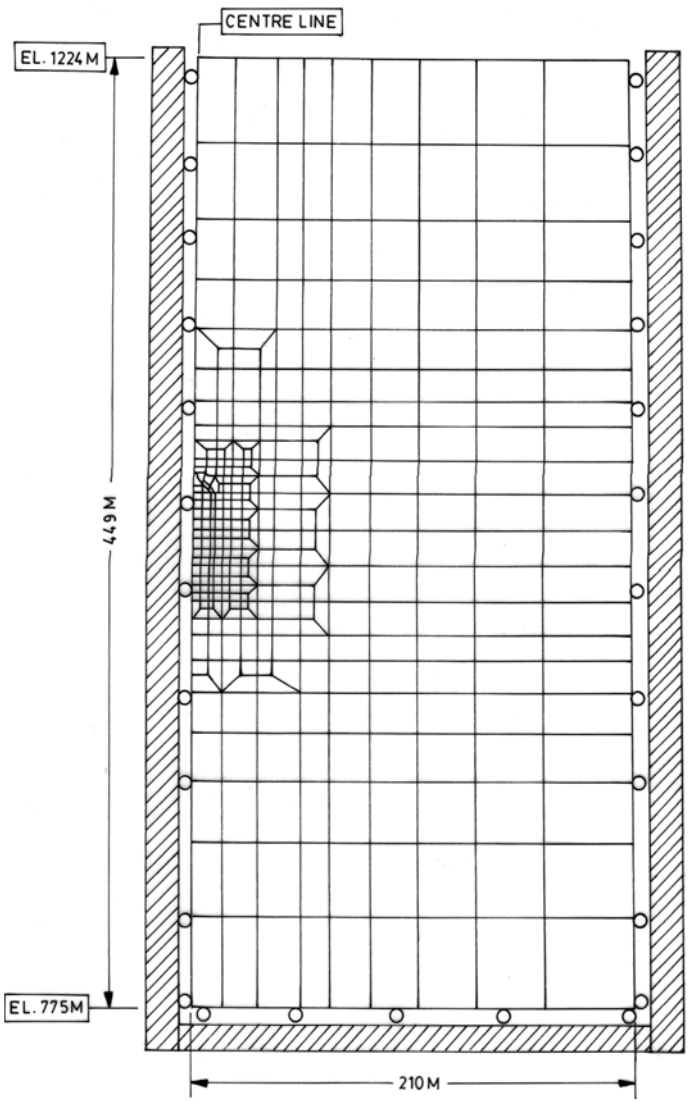

Fig. 18 Finite Element Discretisation

The deformed shape of the cavern and the rock mass is shown in Figure 19. The horizontal displacement contours are shown in Figure 20. Higher movements of the wall are noted around the mid-height of the wall. The maximum value of 42.6 mm movement is observed at the cavern face and this value decreases to 9.22 mm at a distance of 73 m from the face.

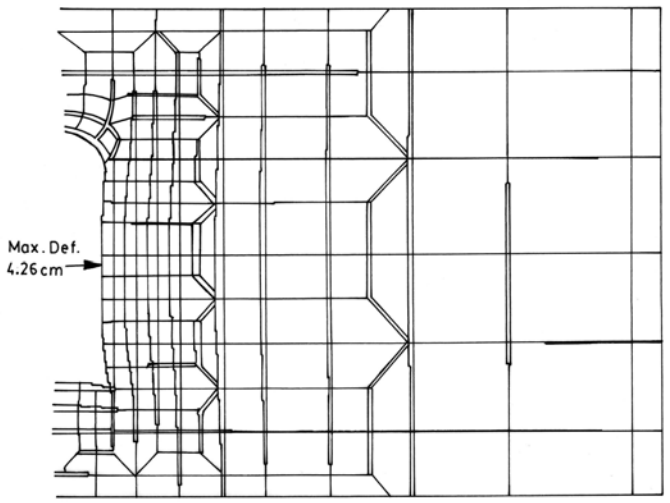

Fig. 19 Deformed Shape of the Cavern and Rock Mass

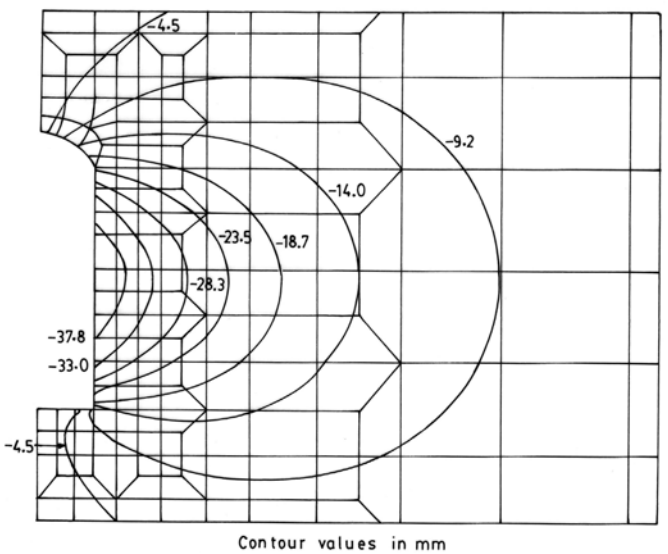

Fig. 20 Horizontal Displacement Contours around the Cavern

The vertical displacement contours are presented in Figure 21. Higher movements are noted around the cavern and the invert portions. The maximum upward movement is 24.2 mm at the invert and it reduces to a value of 7.77 mm at a depth of 18.5 m below the invert. At the crown, the maximum downward movement is 12.68 mm and the value decreases to 4.50 mm at a height of 16.5 m above the crown. The higher vertical movement at the invert portion may be attributed to the large release of in-situ stress and also to the flat geometry of the invert.

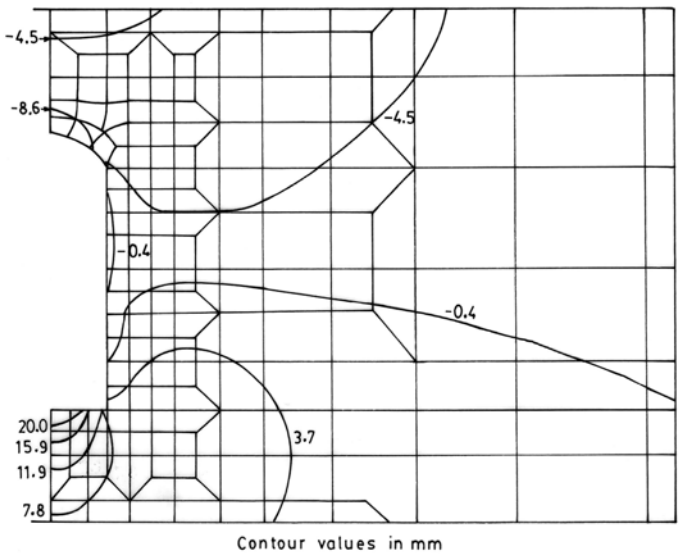

Fig. 21 Vertical Displacement Contours around the Cavern

The major principal stress contours are presented in Figure 22. The maximum value of principal stress is 29.9 MPa. Stress concentration is noted in the corner of the cavern. The minor principal stress contours are shown in Figure 23. As would be expected, along the boundary of the cavern, the stress values are close to zero.

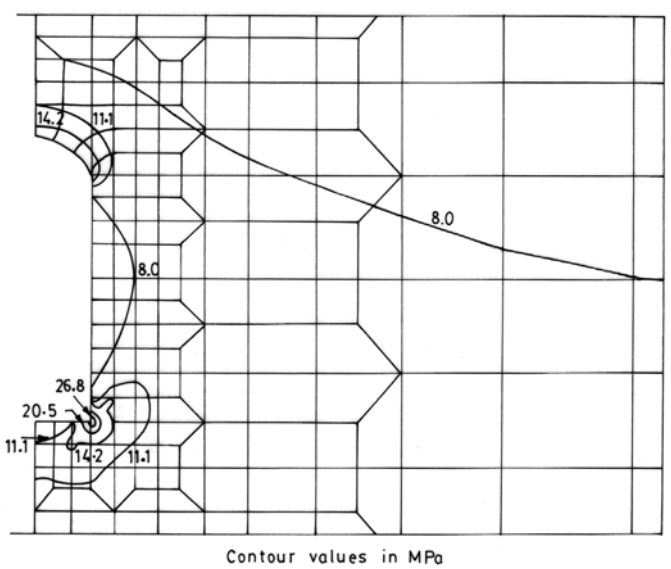

Fig. 22 Major Principal Stress Contours around the Cavern

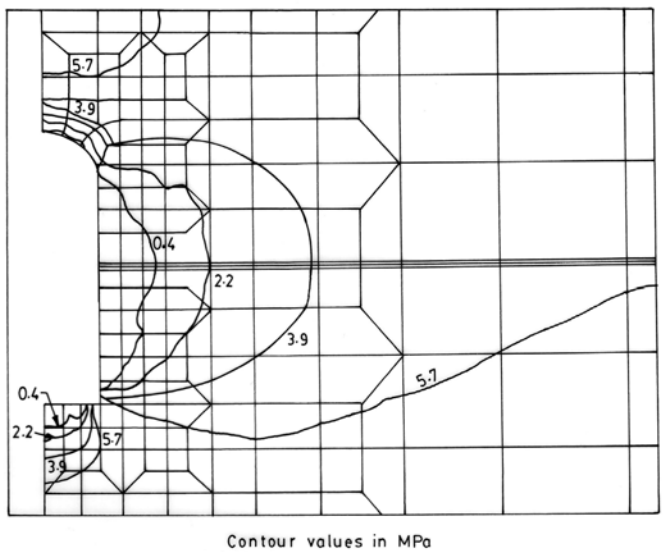

Fig. 23 Minor Principal Stress Contours around the Cavern

The yielding in the rock is noted in the crown and near the corner in the invert. As such the plastic yielding is restricted to very small zone.

The powerhouse cavern has been instrumented by National Institute of Rock Mechanics (NIRM), Kolar using mechanical and remote type extensometers, to study the movement in the rock mass during various stages of excavation (NIRM, 1997). The instrumentation scheme of a section in the middle of the cavern is shown in Figure 24. The instruments at A are installed after the central drift has been excavated. The predicted and observed values of the displacements are presented in Table 5 and are found to be, in general, close to each other.

Table 5 Comparison of Predicted (FEM) and Observed (instrumentation) Deformation at the Powerhouse Cavern Boundary

Stage No.	Excavation Done		Instrumentation at El. (m)	Deformation (mm)	
	From El. (m)	To El. (m)		Predicted (FEM)	Observed (Instrumentation)
1	Widening of the Central drift		1024 (A)	10.4	13-18
2	Widening of the Central drift		1022 (B)	12	6-12
3	1018	1006	1022 (B)	0.6	-1.3 to +2.5
4	1006	1000	1018 (C)	3.5	1-4
5	1000	975	1006 (D)	23.7	10-45
6	983	975	996 (E)	9.4	1-3

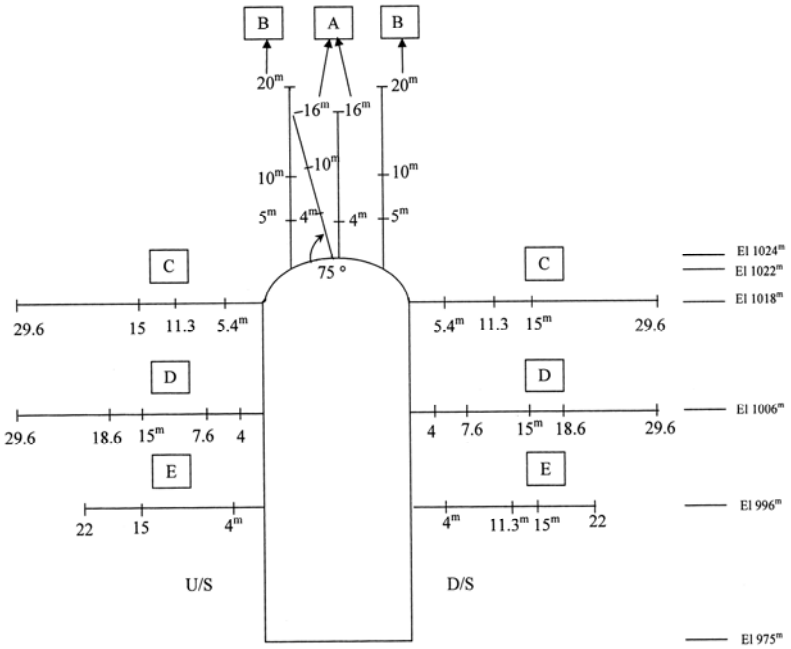

Fig. 24 Instrumentation Scheme at the Middle Section

Analysis of a Circular Tunnel by Equivalent Material Approach

Equivalent material approach can be adopted to characterize the behaviour of rock with well defined joint sets. Zienkiewicz and Pande (1977) and Sharma and Pande (1988) have presented the equivalent material approach for modeling the behavior of jointed rock mass without and with grouted (passive) reinforcement. The equivalent material approach can be used when all joints in a set are parallel and continuous with regular spacing which is small as compared to the overall dimensions of a problem.

The rheological analogue of the reinforced jointed rock mass is shown in Figure 25. It consists of strings which are connected in parallel. Each string consists of units connected in series. Thus, each string will have identical increment of strain equal to that of the equivalent material. The increment of load is shared by the strings in proportion to their volume. The first string in Figure 25 consists of units representing rock material and all the sets of discontinuities, i.e. rock mass. The series connection ensures that the rock material and all the sets of discontinuities will experience the same stress and will have the strains that are additive. Each of subsequent strings (Figure 25) consists of a set of reinforcements and an associated interface set. Herein, it is assumed that there is no relative slip in the reinforcement (i.e., between the bolt and the grout).

In the present paper, the intact rock material is considered to be linearly elastic, isotropic with two elastic constants, viz., Young's modulus, E, and Poisson's ratio, ν. The elastic behaviour of the joints is represented by normal

stiffness (K_n) and shear stiffness (K_s). The yielding of each joint set is governed by the Mohr-Coulomb yield criterion with the restriction that tensile stresses are not permissible in the joints. The passive reinforcement sets considered herein deform to an extent equivalent to the jointed rock mass. The elastic behaviour is represented by two elastic constants, viz., Young's modulus, E and shear modulus, G, and yielding is assumed to be governed by von Mises yield criterion. The joints and reinforcement are considered to exhibit elasto-viscoplastic behaviour. The mechanical properties of a typical set of joints/reinforcement are defined with reference to the local axes of coordinates.

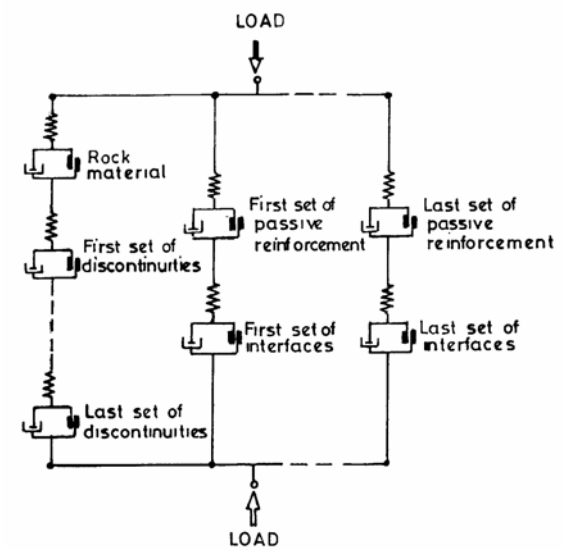

Fig. 25 Rheological Model of Reinforced Jointed Rock Mass

Sharma and Pandya (1988) and Sharma et al. (1989) carried out finite element analysis of a deep circular tunnel of 8 m diameter, excavated in rock mass having a single set of joints inclined at 45^o as shown in Figure 26.

The vertical in-situ stress is assumed as 2.5 MPa and the in-situ stress ratio as 1.0, and two cases, viz.,

Case I: Jointed rock mass without reinforcement

Case II: Jointed rock mass with reinforcement

have been considered in the analysis.

The finite element mesh with 108, 8-noded elements and 348 nodes, is shown in Figure 27. Because of the presence of joints, full section has been discretised. The tunnel has been analyzed for the two cases (Cases I and II) using the material properties as

i. Intact rock

Young's modulus, $E = 2.8 \times 10^4$ MPa
Poisson's ratio, $\nu = 0.2$

ii. Joint set

Normal stiffness, $K_n = 1.0 \times 10^4$ MPa/m
Shear stiffness, $K_s = 0.5 \times 10^4$ MPa/m
Spacing = 0.2, 0.5, 1.0 m
Cohesion, c = 0.07 MPa
Angle of interface friction, $\phi = 45^o$

iii. Reinforcement

Young's modulus, $E = 0.2 \times 10^5$ MPa
Shear modulus, $G = 0.769 \times 10^4$ MPa
Yield strength, $\sigma_y = 250$ MPa
Length of rock bolts = 1 m
Volumetric proportion of reinforcement, $v_r = 0.1\%$.

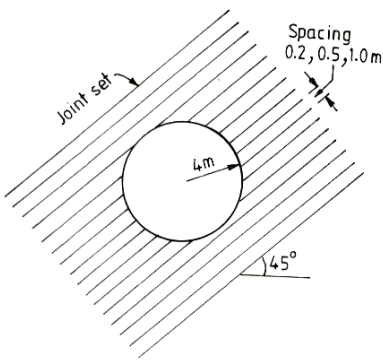

Fig. 26 Circular Tunnel in Jointed Rock Mass

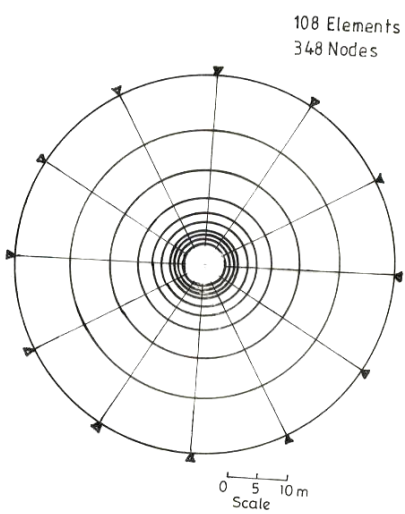

Fig. 27 Finite Element Mesh for Tunnel

Figure 28 shows the displaced shape of the tunnel for the two cases, Case I and Case II for the joint spacing of 0.2 m. The deformation is not concentric though the rock mass is subjected to isotropic stress condition. The presence of the joint set has introduced anisotropic behaviour. In Figure 29 is shown the plot of radial displacements, in parallel and perpendicular directions with respect to the direction of the joint set. It is seen from Figures 28 and 29 that the deformation is more in the direction perpendicular to the direction of the joint set as would be expected for the two cases. This clearly brings out the effect of reinforcement in reducing the displacements in the direction perpendicular to the joint set. Thus the provision of the passive reinforcement results in a significant reduction in deformation. Similar behaviour was observed for other two spacings.

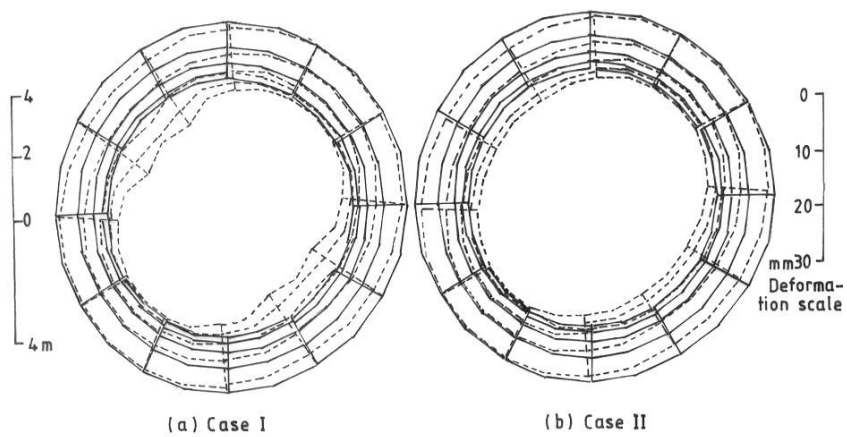

Fig. 28 Deformed Mesh Plot for Joint Spacing of 0.2m

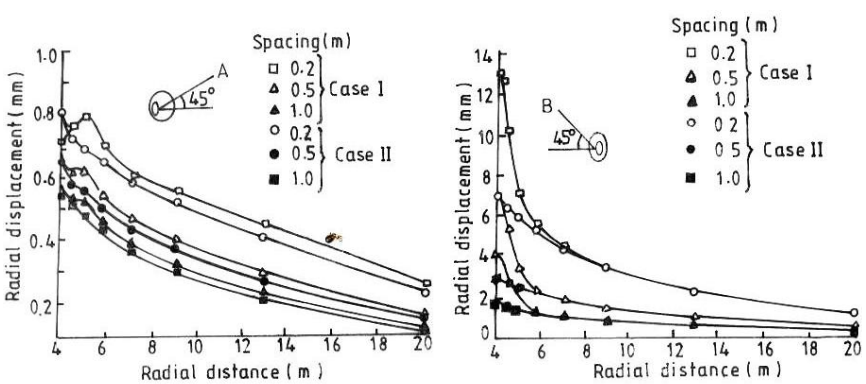

Fig. 29 Radial Displacement along Lines OA and OB

The principal stresses are plotted in Figure 30 along the radial line OC (inclined at 23.6°) passing through the Gaussian points near the springing line for joint spacing of 0.2 m. The major principal stress σ_1 for Case I (without reinforcement) is nearly zero at the tunnel boundary and increases with radial distance in the plastic region, attains a peak value and then decreases with the radial distance. The major principal stress for rock mass with reinforcement (Case II) is approximately equal to 2 MPa on the tunnel boundary and it attains a peak and then decreases with the radial distance. The peak value occurs close to the tunnel boundary for Case II. The minor principal stress σ_3 is zero at the tunnel boundary and increases with the radial distance away from the boundary for both Cases I and II. The rock mass with reinforcement (Case II) shows smoother variation of stress for all the joint spacing.

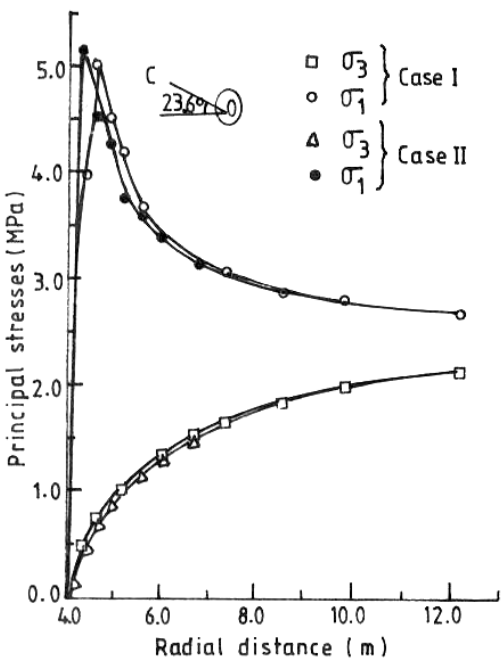

Fig. 30 Principal Stresses along Line OC for Joint Spacing of 0.2m

The axial stress in the reinforcement has been plotted in Figure 31 along Gaussian point lines OD and OE (inclined at 23.6°). The two lines extend up to a radial distance of 5 m since rock bolt length is 1 m. As there is no yielding of the reinforcement along line OD, the axial stress is very small with respect to the yield strength σ_y. As seen from the figure, the axial stress at the tunnel boundary along line OE is equal to the yield strength of the reinforcement (=250 MPa) for all the spacing and the stress decreases with the radial distance. The reduction rate is much lower for joint spacing of 0.2 m and it increases with increase in the joint spacings

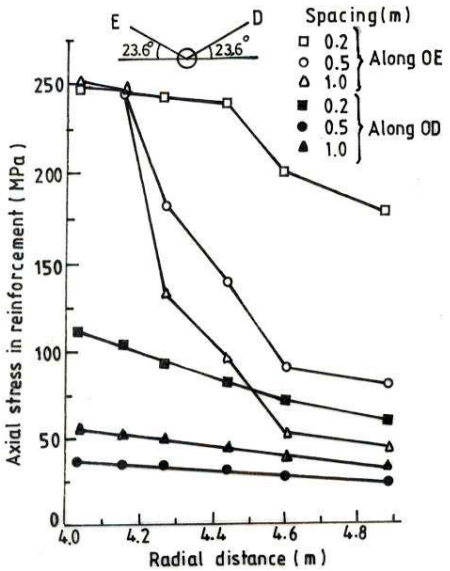

Fig. 31 Axial Stress in Reinforcement along Lines OD and OE

Three-Dimensional Finite Element Analysis of Branching Tunnels

An important component in most hydropower projects is the water carrying pressure tunnel. The network of tunnels in the projects essentially requires their branching at various locations such as the branching of pressure tunnels to feed various generating units, branching of head race tunnel for off-taking vertical surge shaft in the case of underground surge tank, the intersection of adits or shafts with the main tunnel as shown in Figure 32.

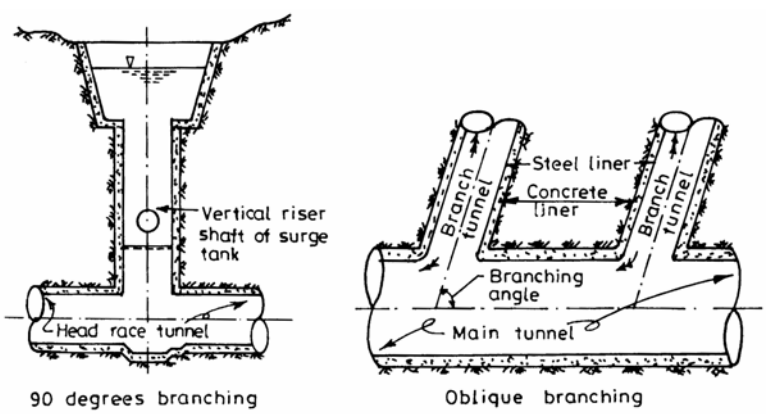

Fig. 32 Typical Examples of Branching Tunnels

Although extensive analysis procedures are available for design of a single tunnel, there is paucity of literature on stress analysis and lining design

for the junction zones associated with the branching tunnels. The simplified design approach in vogue is to ignore the contribution of surrounding rock in sharing the loads from the liners. Thareja (1984) and Thareja et al. (1985, 1986) carried out three-dimensional finite element analysis of circular branching tunnels using 20-noded isoparametric hexahedron elements considering linear elastic behaviour of lining and surrounding rock mass. All aspects of branching tunnels associated with hydropower projects, viz., 90° and oblique branchings, bifurcating and trifurcating tunnels, concrete liners with and without steel liner, steel liner with cracked backfilled concrete, and thickened and normal junctions were considered in the parametric studies. A typical finite element mesh for a trifurcating tunnel with main and branch tunnel diameters of 375 cm and 250 cm, respectively, with their respective concrete lining thickness of 30 cm and 20 cm and 1 cm thick steel liner on its inside surface is shown in Figure 33.

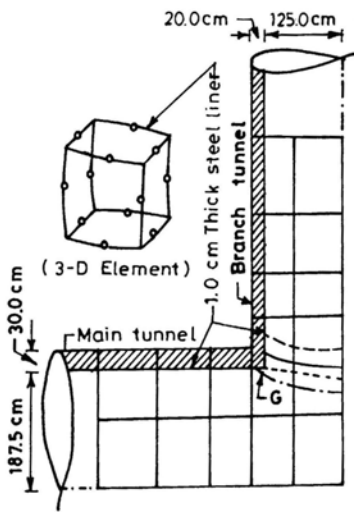

Fig. 33 Discretised Continuum of Steel Lined Trifurcating Tunnel

Analyses were carried out with a hydrostatic pressure of 0.1 MPa (1kg/cm^2) for the complete identified range of dimensions (diameter, liner thickness) of main and branching tunnels and of rock deformation modulus, E_r (Table 6). Rock surrounding the liner was simulated by Winkler model. The necessary theory for implementation of the effect of concrete and steel liners acting independently and together, cracked backfilled concrete and surrounding rock mass was developed. Poisson's ratio of concrete has been taken as 0.25. For steel liner, the modulus value of 2×10^5 MPa and Poisson's ratio of 0.30 have been used.

The contribution of rock participation in relieving the stresses in the liner has been investigated. Table 7 shows the effect of rock participation at junction and at boundary for outside and inside surfaces of concrete liners corresponding to the dimensions of main and branching tunnels of Table 6. It is observed from the table that there is a considerable reduction in stresses at the junction when rock participation in sharing the stresses is considered. Empirical equations were proposed to predict peak hoop stresses. Details of these analyses and equations are given in Thareja (1984).

Table 6 Dimensions of Main and Branch Tunnels and Deformation Modulus of Rock (continued in the next page)

S.No.	D/d ratio	Dimensions (cm)				Deformation modulus of rock, E_r (MPa)
		Main Tunnel		Branch Tunnel		
		Diameter, D	Thickness, T	Diameter, d	Thickness, t	
1	1.5	375.0	30	250	20	250
2	1.5	375.0	30	250	20	500
3	1.5	375.0	30	250	20	1500
4	1.5	375.0	30	250	20	5000
5	2.0	2000.0	60	1000	45	5000
6	2.0	2000.0	60	1000	45	7500
7	2.5	1000.0	45	400	30	1000
8	2.5	1000.0	45	400	30	5000
9	2.5	1000.0	45	400	30	15000
10	2.5	1000.0	45	400	30	30000
11	2.5	1500.0	45	600	30	2500
12	2.5	1500.0	45	600	30	5000
13	2.5	1500.0	45	600	30	7500
14	2.5	1500.0	45	600	30	10000
15	4.5	1462.5	45	325	30	2500
16	4.5	1462.5	45	325	30	12500
17	8.0	2000.0	60	250	20	5000

Table 7 Effect of Rock Participation at Junction and at Boundary for Outside and Inside Surfaces of Concrete Lined Tunnel Branchings

S.No	D/d	E_r (MPa)	%age reduction in hoop stress with respect to rock participation					
			Tunnel Boundary Outside Surface		Outside Junction	Tunnel Boundary Inside Surface		Inside Junction
			Branch	Main		Branch	Main	
1	1.5	250	5.87	5.87	5.28	5.74	5.74	20.08
2	1.5	500	11.05	11.05	9.45	10.90	10.90	31.00
3	1.5	1500	27.46	27.46	23.17	26.95	26.95	50.78
4	1.5	5000	57.34	57.34	53.66	55.96	55.96	75.12
5	2.0	5000	69.61	77.26	80.90	69.13	76.95	86.13
6	2.0	7500	78.27	84.18	86.20	77.64	83.88	90.22
7	2.5	1000	20.97	30.10	23.35	20.56	29.84	40.74
8	2.5	5000	58.71	69.61	64.79	57.50	69.13	77.63
9	2.5	15000	83.71	89.28	85.61	82.08	88.56	91.60
10	2.5	30000	93.71	95.95	94.10	91.81	95.27	96.53
11	2.5	2500	49.89	61.93	60.55	49.43	61.70	69.05
12	2.5	5000	67.54	77.26	75.59	66.92	76.95	82.61
13	2.5	7500	76.47	84.18	81.99	75.76	83.88	87.36
14	2.5	10000	81.93	88.13	86.18	81.18	87.83	90.66
15	4.5	2500	36.09	61.38	52.68	35.07	61.10	63.02
16	4.5	12500	77.02	90.48	86.47	77.02	90.16	92.00
17	8.0	5000	57.34	77.26	72.34	55.96	76.95	72.80

Analysis Using Boundary Element Method

Varadarajan et al. (1983a) used indirect boundary element formulation to analyse three tunnel shapes viz. D-type, horse-shoe and four-arc with same area of cross-section for in-situ stress ratios of K_o = 0.5, 1 and 2. Effect of width to height ratio was also considered in the analysis. It was concluded that the four-arc shaped tunnel indicated better behaviour and in the case of horse-shoe shaped tunnel, better performance was obtained for larger width/height ratio.

Analysis of a Powerhouse Cavern

As a part of Subansiri hydropower project in North East India, a D-shaped power house cavern (24 m wide, 43 m high and 320 m long) located at 187 m from the ground surface is proposed to be constructed in a sandstone rock formation. Varadarajan and Sharma (1984b) carried out the two-dimensional elastic analysis of the powerhouse cavern using BEM by discretising the cavern into 34 boundary elements for two values of in-situ stress ratio, K_o = 0.5 and 1.0. The properties of the rock are:

Young's modulus, $E = 3 \times 10^6$ kPa,

Poisson's ratio, $\nu = 0.20$, and

Unit weight, $\gamma = 25$ kN/m^3.

The in-situ stresses in the cavern corresponding to the overburden of 187 m are 4675 kPa in the vertical direction and 2337.5 kPa in the horizontal direction for K_o = 0.5. The stresses and displacements obtained from the analysis for K_o = 0.5 have been plotted and are presented in Figure 34. In the crown, the displacement is downward with maximum displacement of 28 mm. The side walls move inward with maximum movement being 24 mm at the mid-height of the wall. The floor heaves due to the excavation and the maximum displacement of 48 mm occurs near the centre. The major and minor principal stress contours show stress concentration in the corner near the crown and near the floor.

Analysis Using Coupled FEBEM

The finite element method (FEM) and the boundary element method (BEM) are two well established numerical methods used for the analysis of underground openings. The advantages of both the methods are utilised by adopting FEBEM in which finite elements are coupled with boundary elements. Some aspects of coupled FEBEM analysis of circular and D-type openings have been investigated by Singh (1985), Varadarajan et al. (1983b, 1985a & b, 1987) and Singh et al. (1985, 1988, 1989).

For the condensation of boundary element stiffness matrix, the procedure proposed by Sharma et al. (1985a) has been adopted. Both elastic and elasto-plastic analyses were carried out using plane strain condition. The results are presented here for circular opening.

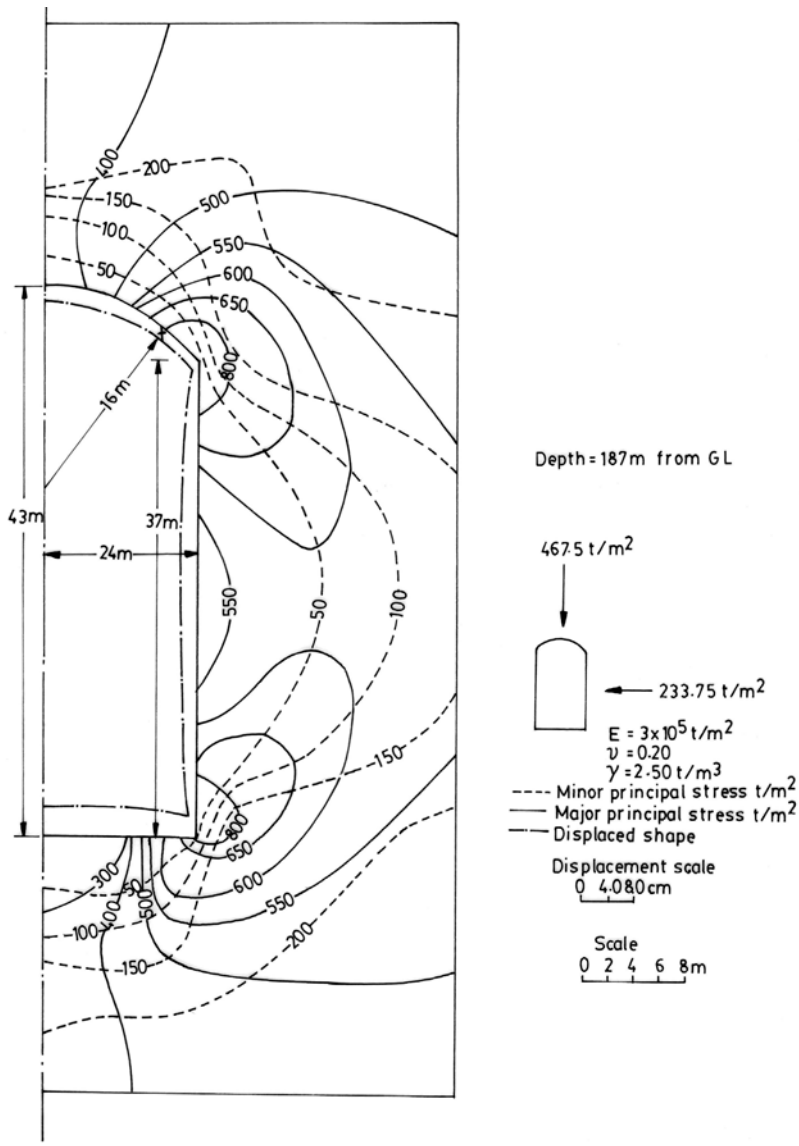

Fig. 34 Deformed Shape and Principal Stress Contours for Powerhouse Cavern

Figure 35 shows a FEBEM discretisation for linear elastic analysis. The effects of the location of interface boundary between finite and boundary elements, the Poisson's ratio and the stress ratio are studied. A constant value of Young's modulus E equal to 1 MPa is taken for all the cases. The value of Poisson's ratio ν is varied from 0.0 to 0.49. Three insitu stress ratios viz. K_o = 1.0, 0.5 and 0.0 are used. The loading due to the excavation of the tunnel is applied.

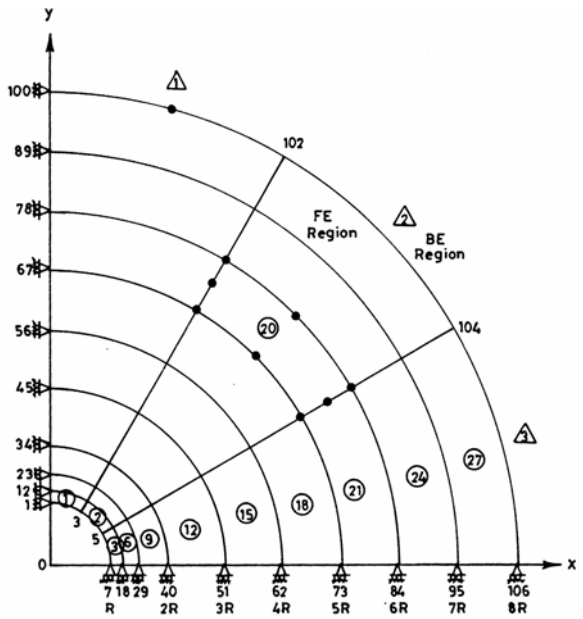

Fig. 35 FEBEM Discretisation for Different Interface Locations between FE and BE Regions

The effects of the interface boundary location and the value of the Poisson's ratio on the radial displacement u_R for $K_o = 1$ are given in Table 8. It is found that the location of the interface boundary between FE and BE at two times the width of the opening provides accurate results. The Poisson's ratio has significant effect on the accuracy of the results.

Table 8 Radial Displacement u_R at the Boundary of the Opening (FEBEM), $K_o = 1.0$

u_R by CFS	0.0100		0.01250		0.01450		0.01490	
ν	0.0		0.25		0.45		0.49	
Boundary distance	u_R	%age error	u_R	%age error	u_R	%age error	u_R	%age error
2R	0.010037	0.370	0.012596	0.768	0.015904	9.683	0.014766	-0.899
3R	0.010013	0.130	0.012523	0.184	0.014674	1.200	0.019049	27.845
4R	0.010008	0.080	0.012511	0.088	0.014535	0.241	0.015415	3.456
5R	0.010008	0.080	0.012510	0.080	0.014514	0.097	0.014960	0.403
6R	0.010008	0.080	0.012510	0.080	0.014512	0.083	0.014911	0.074
7R	0.010008	0.080	0.012510	0.080	0.014512	0.083	0.014936	0.242
8R	0.010008	0.080	0.012510	0.080	0.014513	0.090	0.014968	0.456

CFS – closed form solution

The effect of insitu stress ratio K_o on radial displacements for Poisson's ratio of $\nu = 0.25$ is presented in Table 9. It is observed that the stress ratio causes slight increase in the error of the results. The displacements and stresses predicted by FEBEM are more accurate than by FEM.

Table 9 Effect of Stress ratio on Radial Displacements ($\nu = 0.25$)

Location	In-situ stress ratio, K_o	u_R by CFS	FEBEM		FEM	
			u_R	%age error	u_R	%age error
Springing	1.0	0.012500	0.012511	0.088	0.011941	-4.472
Crown		0.012500	0.012511	0.088	0.011941	-4.472
Springing	0.5	0.003125	0.003229	3.328	0.003267	-4.544
Crown		0.015625	0.015538	-0.557	0.014645	-6.272
Springing	0.0	0.006250	0.006053	-3.152	0.005407	-13.488
Crown		0.01875	0.018564	-0.992	0.017348	-7.477

CFS – closed form solution

To study the effect of insitu stress ratio on yielded zone, displaced shape and principal stresses, an elasto-plastic analysis of a circular underground opening using the FEM and FEBEM has been carried out. The discretisation schemes used for FEBEM and FEM are shown in Figure 36.The Mohr-Coulomb yield criterion has been adopted. The material properties are shown in Table 10. The interface between FE and BE is taken at four times the radius of the opening and the yielding is confined to the FE region.

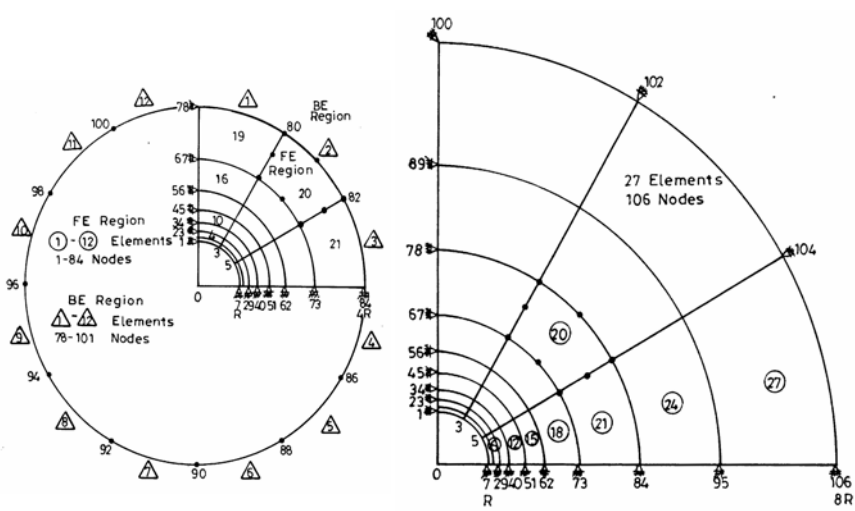

Fig. 36 Discretization of Circular Opening by FEBEM and FEM

Table 10 Rock Properties

Properties	Value
Young's modulus, E	4.48×10^5 kPa
Poisson's ratio	0.18
Cohesion, c	16.0 kPa
Angle of internal friction, ϕ	41°
Unit weight, γ	29.4 kN/m^3
Permissible tensile strength, σ_t	8.5 kPa
Height of overburden, h	300 m

The yielded zones and displaced shapes are shown in Figure37 and 38, respectively. It is found that the stresses predicted by FEBEM are more in the elastic analysis and more accurate (Varadarajan et al., 1985b). In the elasto-plastic analysis, both FEM and FEBEM predict almost same stresses in the plastic zone. The stress reduction due to yielding is, therefore, more for FEBEM. This leads to larger yielded zone and greater displacements in the case of FEBEM (Figures 37 and 38). For the field problem with extensive yielding, FEBEM which contains less number of equations may be computationally economical.

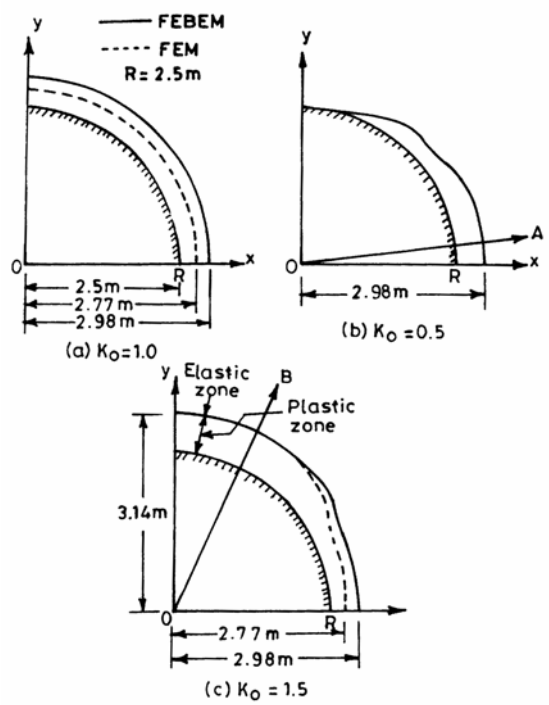

Fig. 37 Yielded Zones by FEBEM and FEM for Different Stress Ratios

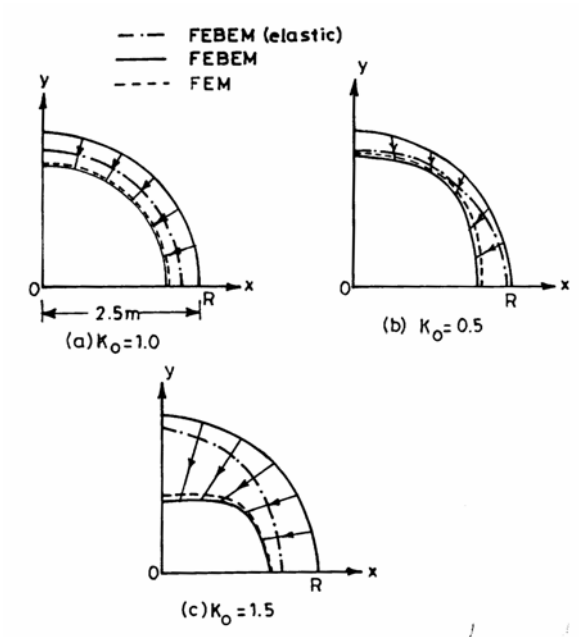

Fig. 38 Displaced Shapes by FEBEM and FEM for Different Stress Ratios

Analysis of Delhi Metro Tunnels in Alluvium using FLAC

Phase I of Delhi Metro Rail project has been completed with 13.7 km of underground, 47.5 km of elevated and 4.5 km on surface corridors. Out of 13.7 km of underground corridor, tunnels have been driven in Delhi silt (alluvium) in three areas viz. Kashmere Gate to Chandani Chowk (B1), New Delhi Railway Station to Rajeev Chowk (B4) and Rajeev Chowk to Patel Chowk (B6) using Earth Pressure Balance Machine (EPBM). The segmental linings of 28 cm thickness made of M45 grade concrete were erected inside the cylinder (tail skin) as machine advanced to have finished internal diameter of 5.7 m. The annular space left between the outer surface of liners and excavated boundary was grouted through the tail skin. The lining interacts with the ground as it comes into contact due to advancement of the machine.

Tunnels have been analysed for the three areas viz. B_1, B_4 and B_6 considering four sections in each area by Yadav (2005). The sections have been considered corresponding to the monitoring locations, and the general arrangement of settlement markers at these sections is shown in Figure 39. The sections considered for the study have been assigned identification numbers 1, 2, 3, 4; 5, 6, 7, 8; and 9, 10, 11, 12 in B_1, B_4 and B_6 areas, respectively.

Assuming that the full annular space is not filled by grout, the maximum annular gap considered for the present work is 80 mm. With this, the diameter of excavated boundary becomes 6.4 m. The corresponding face loss in the percentage of over-excavated volume with respect to the theoretical excavation up to the outer diameter of liner for 1 m of the tunnel length works out to be 5%.

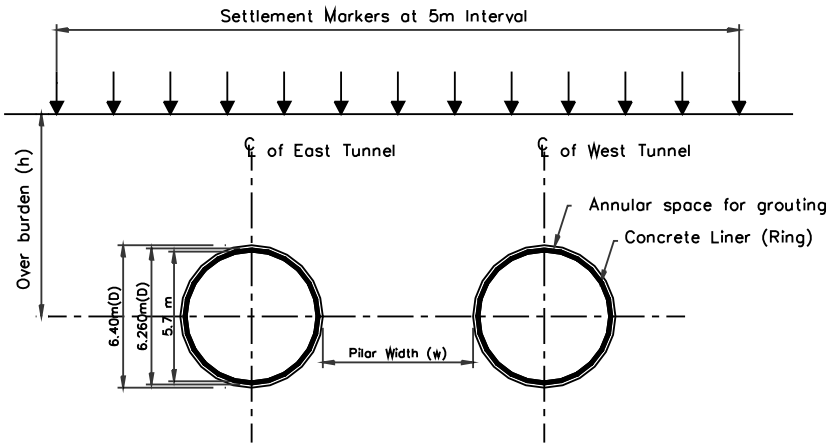

Fig. 39 Settlement Markers Arrangement at Monitoring Lines

Yadav (2005) carried out elasto-plastic analysis of Delhi metro tunnels, assuming plane strain condition, for different face losses using FLAC software (FLAC, 2002) using the properties of Table 11 (DMRC, 2002). The discretization is shown in Figure 40.

Table 11 Parameters for the Sections at Reference Lines in B_1, B_4 and B_6 areas

Reference Line	Cover above the Crown (h) m	Pillar Width (w) m	Young's Modulus (E) MPa	Other Parameters
1	11.70	11.20	1.22 + 0.83z where z is depth measured from the ground level in meters	Cohesion (c) = 0 Friction (ϕ) = 35° Dilation (ψ) = 5° Water Table considered below invert of tunnel (dry condition) Density (γ_{dry}) = 1800 kg/m^3 K_o = 0.5
2	12.80	11.20		
3	10.50	10.40		
4	10.80	9.60		
5	10.8	8.0	1.27 + 0.78z where z is depth measured from the ground level in meters	
6	11.0	7.2		
7	11.3	7.2		
8	13.4	7.2		
9	14.2	7.74	1.27 + 1.14z where z is depth measured from the ground level in meters	
10	13.9	8.74		
11	13.4	8.00		
12	10.6	7.74		

The two vertical boundaries are restrained in x-direction and the bottom horizontal boundary is restrained in vertical direction. The excavation of the tunnels has been done sequentially. The east tunnel is excavated first followed by the excavation of the west tunnel (Figure 40). For the simulation of face loss, the internal radius of the liner has been adjusted to accommodate the desired

gap between the liner and excavated boundary keeping the radius of the excavation as 3.2 m. The face losses of 2, 3, 4 and 5 percent have been taken for the analysis. The gap provided between the liner and excavated boundary is 32, 48, 64 and 80 mm for the face loss simulation of 2, 3, 4 and 5 percent respectively in the present work.

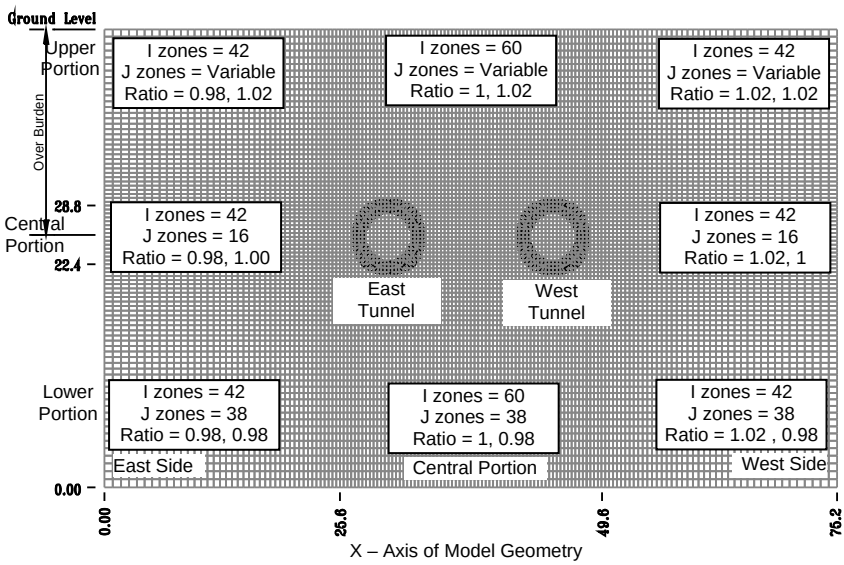

Fig. 40 Mesh adopted for Analysis of Tunnels in Alluvium

The maximum ground surface settlement, maximum axial force and maximum bending moment in the liners at these sections, obtained from the analysis after excavation of both tunnels sequentially, are presented in Table 12.

Table 12 Maximum Surface Settlement, Axial Force and Bending Moment at Different Sections in B_1, B_4 and B_6 Areas

Parameters		Sections														
		1	1	1	1	2	3	4	5	6	7	8	9	10	11	12
Percentage Face Loss		2	3	4	5	4	4	4	4	4	4	4	4	4	4	4
Settlement (mm)	1st (excavated first)	11	19	27	35	26	28	28	28	29	30	30	28	28	25	25
	2nd (excavated later)	10	18	25	33	25	26	27	28	29	29	30	29	27	23	22
Max. Axial Force (kN/m)		638	635	635	633	663	586	597	600	610	630	720	750	731	716	596
Max. Moment (kN-m/m)		226	233	243	254	250	232	234	230	240	245	260	265	256	260	227

For Section 1 the results are tabulated for face losses 2, 3, 4 and 5 percent and for other sections the results are given for face loss of 4 percent. The maximum ground surface settlement varies from 11 to 35 mm for change in face loss from 2 percent to 5 percent at Section 1 for the tunnel excavated first. It is observed that there is an influence on the first tunnel due to the excavation of the second tunnel.

The settlement troughs were plotted for different face losses and were compared with field measurements from settlement markers. The typical settlement trough at the ground surface after excavation of both the tunnels at Section 6 in B4 area is presented in Figure 41. It has been found that the face loss incurred during tunnelling of Delhi Metro in alluvium is of the order of 2 to 4 percent.

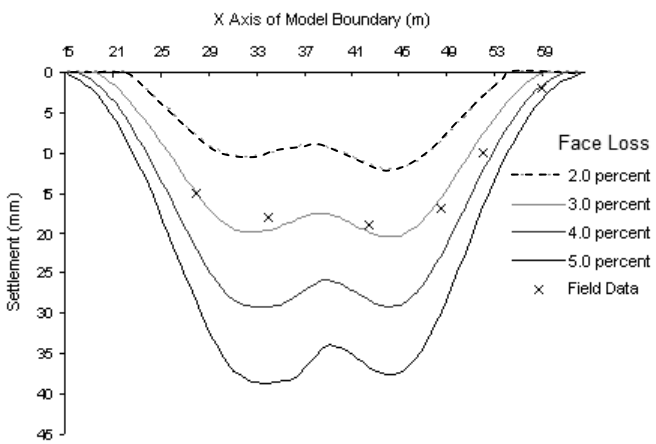

Fig. 41 Settlement Troughs at Section 6 in B_4 Area

The correlations have been developed for prediction of maximum ground surface settlement, and structural forces in the liner, viz. maximum axial force and maximum bending moment, on the basis of parametric study for Delhi Metro. Details of these analyses and correlations are given by Yadav (2005).

Rock-Support Interaction Analysis Using FLAC

Rock-support interaction analysis is very important in the design of tunnels. The analytical solutions are available only for deep circular tunnels in rocks having hydrostatic insitu stress condition ($K_o = 1$) to obtain ground reaction curve (GRC) and support reaction curve (SRC). RocSupport software (Rocscience, 2006) has been developed based on these analytical solutions. Rock-support interaction analysis of circular, horse-shoe and D-shaped tunnels was carried out using FLAC software (Archana, 2007). In the present paper, analysis and results are presented for a deep circular tunnel of 7 m diameter located at a depth of 500 m below ground level using Mohr-Coulomb yield criterion for insitu stress ratios of $K_o = 0.5$, 1.0 and 2.0. Shotcrete has been used as the support system. GRC and SRC are plotted. The results are compared with those from RocSupport software for $K_o = 1$.

The following rock and shotcrete properties were used in the analysis:

(i) Rock

Density = 2600 kg/m^3

Young's modulus (E) = 20 GPa

Poisson's ratio (v) = 0.2

Internal friction angle (ϕ) = 30°

Tensile strength of rock mass = 2 kPa

Cohesion (c) = 3.2 MPa

(ii) Shotcrete

Thickness = 200 mm

Young's modulus (E) = 28 GPa

Poisson's ratio (v) = 0.2

Due to symmetry, half the section of 50 m width and 100 m height around the circular tunnel is considered for discretization as shown in Figure 42 (a).

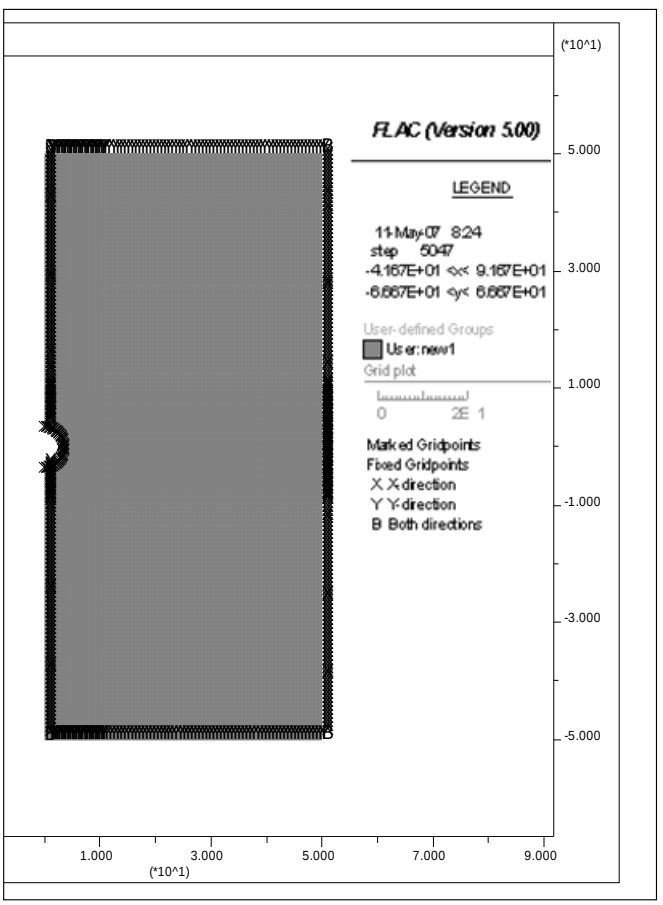

Fig. 42 (a) Mesh for Circular Tunnel

The finer mesh near the tunnel is taken so that the results obtained are more accurate and Figure 42 (b) shows the mesh near the tunnel boundary. For the boundary conditions, the bottom and top are restrained in y-direction and the left and right sides are restrained in x-direction. Corresponding to depth of 500 m, the vertical insitu stress is 12.75 MPa, which is applied uniformly in vertical direction. The corresponding horizontal stress, applied uniformly in lateral direction, is 6.375 MPa, 12.75 MPa and 25.5 MPa for K_o = 0.5, 1.0 and 2.0, respectively.

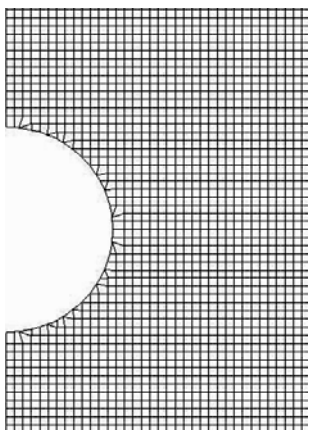

Fig. 42 (b) Mesh near the Tunnel Boundary

Elasto-plastic plane strain analysis of circular tunnel is carried out assuming single stage excavation, but the excavation load is released gradually in steps. Initially when no load is released, the support from the inside rock is 100% on the tunnel boundary. When the full excavation load is released, there is no support from the inside rock. The displacements will go on increasing with the gradual release of the tunnel loads and finally the displacements at full release of tunnel load are determined. The displacements of crown and invert are the same because of symmetry, therefore, the ground reaction curves (GRC) are plotted for the crown and side wall.

Another analysis is carried out to develop support reaction curves (SRC). The support (shotcrete) is assumed to be provided when 36% of excavation load is released and for the remaining release of 64% of excavation load, there will be interaction of rock and support. The displacement at crown and side wall for 36% release of load is one point of SRC with no support pressure. The other point is when remaining 64% load is released. The two points are joined by straight line assuming linear elastic behaviour of support system. The equilibrium point will be the intersection point of GRC and SRC and the tunnel will have the final displacement and support pressure at crown and springing corresponding to this point.

Following the above procedure, the GRC and SRC for K_o = 0.5, 1.0 and 2.0 are plotted in Figures 43 to 45, respectively and the results are summarized in Table 13. The displacement obtained after full release of load at the crown, invert and springing is 3.39 mm for K_o = 1. At the equilibrium point, where the support curve and GRC intersects, the displacement is 2.60 mm and the support

pressure is 0.12 MPa. From the RocSupport software, the corresponding displacement and support pressure are obtained as 2.62 mm and 0.10 MPa, respectively. The two results match closely.

The curve for the springing has shifted to right with respect to the curve for the crown for $K_o = 2.0$, whereas for $K_o = 0.5$, the curve for the springing has shifted to left.

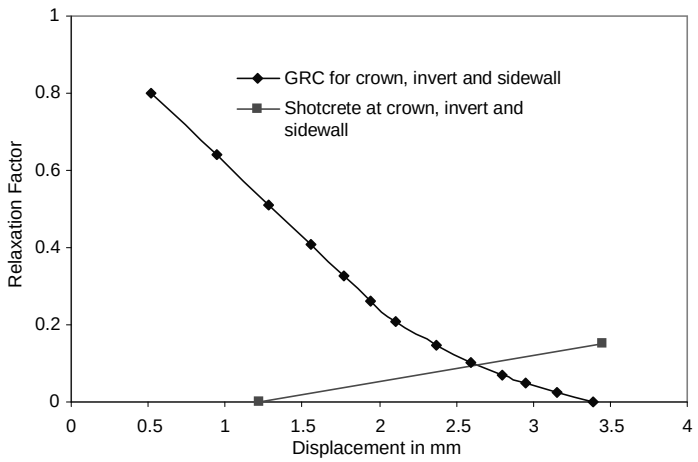

Fig. 43 GRC and SRC for Circular Tunnel for $K_o = 1.0$

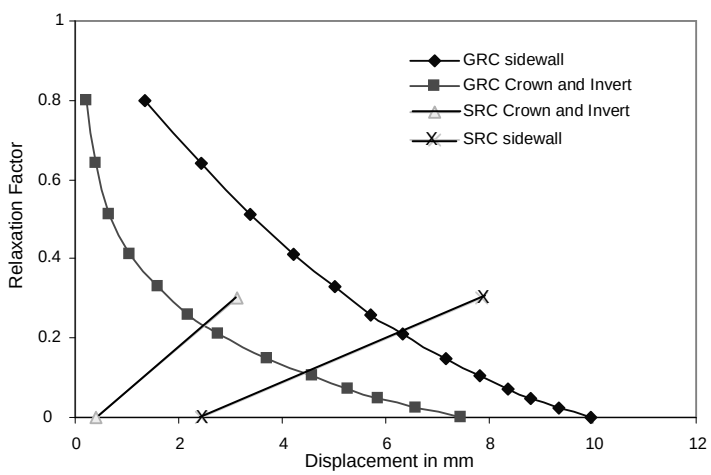

Fig. 44 GRC and SRC for Circular Tunnel for $K_o = 2.0$

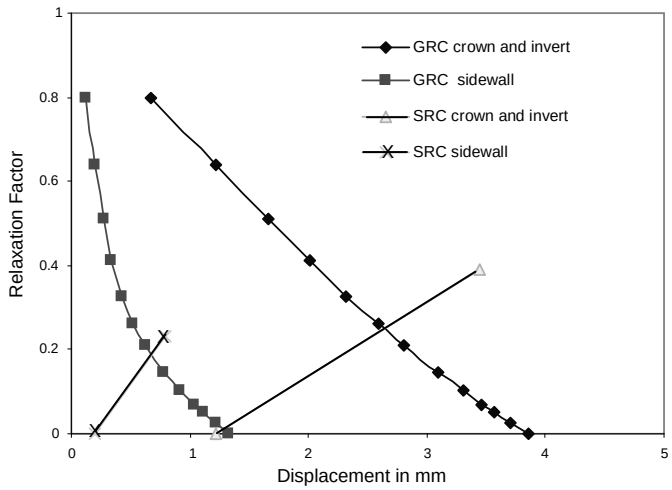

Fig. 45 GRC and SRC for Circular Tunnel for $K_o = 0.5$

Table 13 Final Wall Displacements after Support Installation

Insitu Stress Ratio	Supports	Crown (mm)	Invert (mm)	Springing (mm)	Axial stress in shotcrete (MPa)
$K_o = 1$	Without support	-3.39	3.39	3.39	
	With shotcrete	-2.82	2.82	2.82	3.07
$K_o = 2$	Without support	-7.47	7.47	-10.20	
	With shotcrete	-3.13	3.13	-7.84	11.12
$K_o = 0.5$	Without support	-3.90	3.90	-1.33	
	With shotcrete	-3.45	3.45	-0.80	4.16

Analysis of Underground Nuclear Repository

Nuclear waste storage structures are completely encased and housed into the existing host ground medium. Unlike a surface structure, interaction of the host medium with the underground structure plays an important role in the proper design of an underground structure. Nuclear waste consists of radionuclides which have extremely long half life and high heat generation capacity. Therefore, long term performance is very important for the host ground medium of repository structure. The storage concept known as KBS3 concept is used herein.

KBS3 method for disposing of spent nuclear fuel is based on the use of multiple barriers to prevent radionuclides from reaching the ground surface, thus protecting man and the environment from their harmful effects (Pusch, 1994). In its basic configuration, the deep repository consists of a descent tunnel, shaft, central area and a number of deposition tunnels, as shown in Figure 46 (TR, 2004). In each deposition tunnel, there are a number of

deposition holes. The method involves encapsulating the fuel in copper canisters which are then deposited, surrounded by a buffer of bentonite clay, in deposition holes in a tunnel system at a depth of approximately 400–700 m in crystalline bedrock as shown in Figure 47 (TR, 2004).

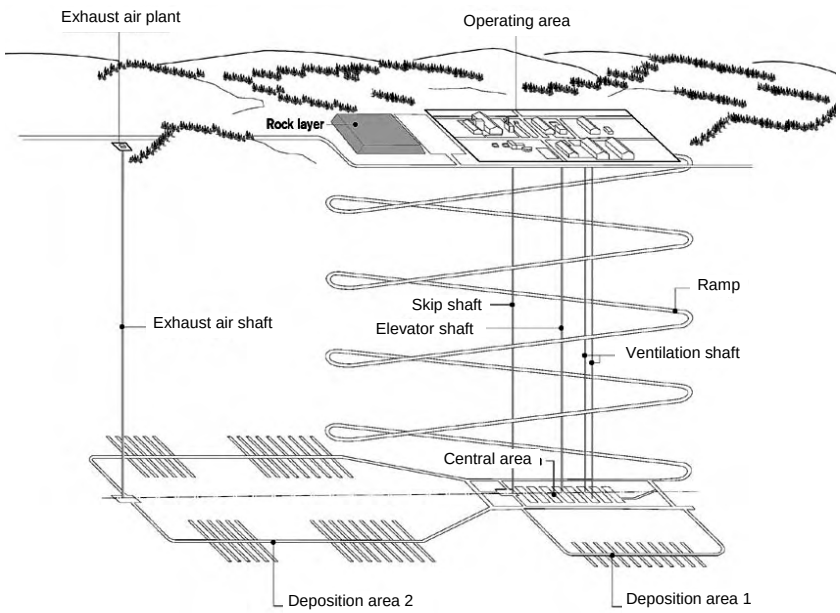

Fig. 46 Schematic Diagram of Deep Repository (TR, 2004)

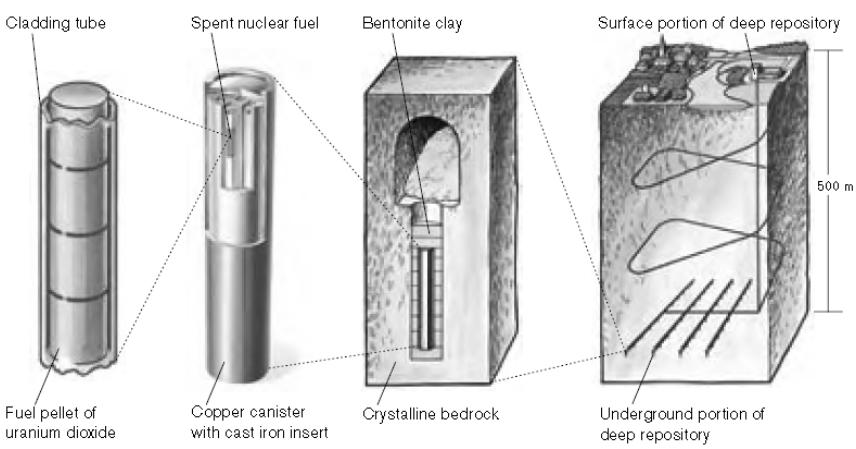

Fig. 47 Multiple Barrier Concept of KBS3 Type Nuclear Repository (TR, 2004)

The location of the deposition tunnels, as well as the spacing between the deposition holes is determined, above all, by the consideration that the temperature on the canister surface may not exceed 100°C. After the canisters have been emplaced in the deposition holes, surrounded by impervious bentonite clay, the tunnel is backfilled with a mixture of bentonite clay and crushed rock. Other chambers are also backfilled when all fuel has been deposited.

At IIT Delhi, two-dimensional finite element analysis of KBS3 and AECL models of nuclear repository using ABAQUS package (ABAQUS, 2004) was carried out (Chakraborty, 2004; Aman Kumar, 2005; Jain, 2006; Chakraborty and Sharma, 2006; Sharma, 2006 & 2007). Three-dimensional analysis of KBS3 type nuclear repository using FLAC3D software (FLAC3D, 2002) was conducted (Patel, 2008; Patel and Sharma, 2008). Transient heat transfer (HT), mechanical (M), thermo-mechanical (TM) and thermo-hydro-mechanical (THM) analyses were carried out for initial temperature values of 25.0°C and 56.6°C and two in-situ stress ratios of K_o = 1.0 and 1.5. In the present paper, typical results from three-dimensional analysis (Patel, 2008) are presented for initial temperature of 56.6°C and K_o = 1.0.

Model Description

The geometric details of deposition tunnel, deposition hole, canister, bentonite and concrete plug of the nuclear repository are shown in Figure 48. The deposition tunnel is of 5 m in height and 5 m in diameter. The deposition hole is of 5 m depth and 1.08 m in diameter. A canister has been placed in the deposition hole. The height of the canister is 1.9 m and diameter 0.36 m. In between canister and deposition hole wall, 0.36 m thick bentonite has been placed. Below the canister, 1.55 m thick bentonite and above canister, 1.45 m thick bentonite has been provided followed by 0.1 m thick concrete plug at the top.

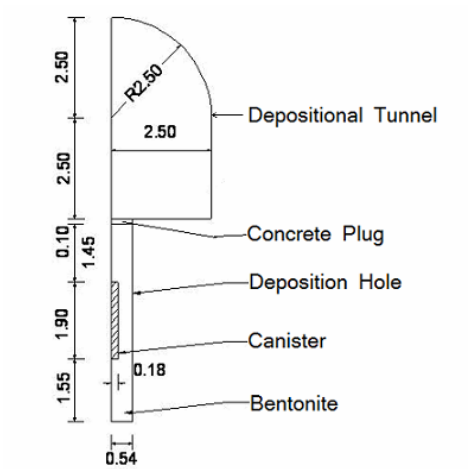

Fig. 48 Details of Deposition Tunnel and Deposition Hole (Dimensions in Meters)

The deposition tunnels are taken at a spacing of 40 m and deposition holes at a spacing of 6 m as shown in Figure 49. The model size (the shaded area of the figure) has been taken as 20 m×3 m×40 m, with one half

of deposition tunnel and deposition hole (because of symmetry, only quarter portion is considered). The effective vertical and horizontal in-situ stresses in rock, corresponding to depth of 500 m from ground level and K_o = 1.0, are taken as 12.5 MPa.

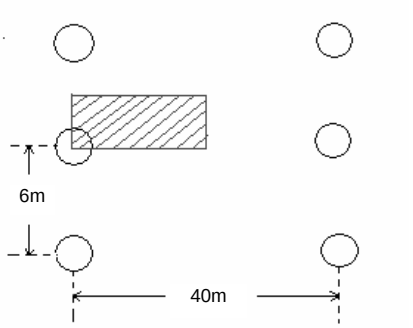

Fig. 49 Top View of the Deposition Hole and the Part Considered for Analysis

For the transient analysis, the heat flux per unit volume, Q, is taken as

$$Q = Q_0 \, e^{-\lambda t},$$

where Q_0 is initial heat flux per unit volume, λ is decay rate and t is the time.

For the present analysis, Q_0 = 2500 Joule/second/m^3 (watt/m^3), λ =7.325x10^{-10}/sec and time t is in seconds. With this data, for time t = 6.3072x10^9 seconds (200 years), Q = 24.63 watt/m^3. The initial temperature of canister and rock is considered as 56.6°C. For thermo-hydro-mechanical analysis, an initial pore pressure of 1.35 MPa is considered, which corresponds to water head of 135 m. All the materials i.e. canister, concrete, bentonite and rock are considered elastic. Table 14 shows the material properties taken for the analysis.

Table 14 Properties of Different Materials

Properties	Bentonite	Canister	Concrete	Rock
Density (kg/m^3)	1610	8913	2500	2581
Thermal conductivity (W/m/°C)	0.5	390	4.0	3.3
Specific heat (Joule/kg/°C)	732	500	800	900
Porosity	0.231	0.001	0.167	0.167
Coeff. of linear expansion (/°C)	1x10^{-6}	1.7x10^{-5}	1x10^{-5}	1.4x10^{-6}
Young's modulus (MPa)	50	109000	250000	29000
Poisson's ratio	0.40	0.36	0.20	0.23
Permeability (m/s)	1x10^{-6}	0	1x10^{-10}	1x10^{-12}
Thermal expansion coefficient	1.48 x10^{-4}	5.16 x10^{-5}	1.3 x10^{-4}	1.08 x10^{-4}

Discretisation

The problem was analyzed using the software FLAC3D. The mesh is shown in Figure 50. Total number of grid points was 5067 and total number of zones was 4152. There were 60 elements in the canister portion, 72 elements in bentonite part, 12 elements in concrete plug and rest in rock medium. The left and front boundaries were assumed to be impermeable for heat and fluid flow, whereas the temperature and pore water pressure at top, bottom, right and back boundaries were fixed. The left, front, back and bottom boundaries were restrained in X-, Y-, Y- and Z- directions respectively. The results in tables are presented corresponding to the points as shown in Figure 51.

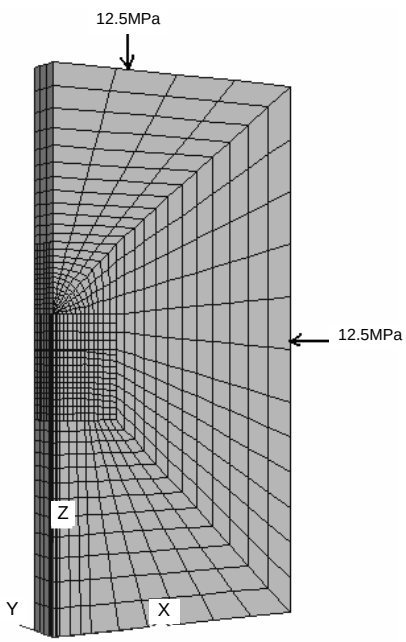

Fig. 50 Finite Difference Mesh and Loading

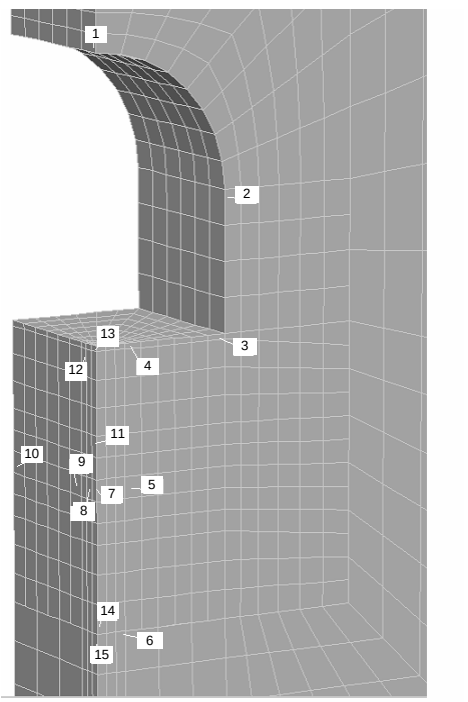

Fig. 51 Points for which Results are presented

Transient Heat Transfer Analysis

For the transient heat flow analysis, the ambient temperature was taken as 56.6°C. Figure 52 shows the plot of the temperature of the repository with time for 200 years at point 8 (corresponding to location of maximum temperature in repository) and point 9 (corresponding to location of maximum temperature in rock), and the maximum temperature obtained was 121°C and 74°C at points 8 and 9 respectively at 10 years after the canister was emplaced. The temperature reaches ambient value of 56.6°C after around 150 years.

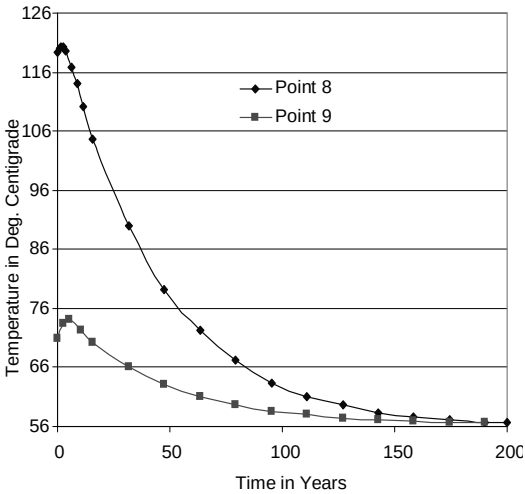

Fig. 52 Temperature Variation at Points 8 and 9 for 200 years

Transient Thermo-Hydro-Mechanical Analysis

As the temperature of the repository was maximum after about 10 years of deposition, the thermal stress generated due to the temperature change is maximum at this time. Therefore, the transient thermo-hydro-mechanical analysis was conducted for 10 years with the ambient temperature of 56.6^{o}C and K_o of 1.0 using a time step of 7200 sec.

Figure 53 shows the pore water pressure distribution due to the thermo-hydro-mechanical coupling. There was a high amount of stress generated due to the temperature change in the repository. Figure 54 shows the X-displacement contours, the maximum being 1.55 mm at point 2. Figure 55 shows the Y-displacement contours with a maximum value of 0.61 mm. Most of the points were moving in the positive Y-direction. Z-displacement contours are shown in Figure 56.

Figures 57 and 58 show the major and minor principal stress contours. It is seen that there is a high compressive stress generated due to the temperature change and the corresponding change in pore water pressure. The maximum value of the major principal stress was found to be 152.6 MPa (compressive). The maximum value of the compressive stress generated in bentonite was 25 MPa at point 14. The maximum value of tensile stress was 6.6 MPa at point 12. There was a high value of tensile stress developed in the concrete near the concrete-rock interface. Due to this high amount of tensile stress the concrete will crack and the pore water pressure will be released. An elasto-plastic analysis can be conducted for that. Table 15 shows the results of the thermo-hydro-mechanical analysis.

The comparison of stress values for the three cases, viz. mechanical (M), thermo-mechanical (TM) and thermo-hydro-mechanical (THM), is presented in Table 16. The compressive stress is given in negative. At the points on the free

surface (tunnel boundary), the major principal stress values decreased due to thermal expansion of the rock. Comparing results of TM and THM cases, it is seen that there is a very high stress generated due to the change in pore water pressure.

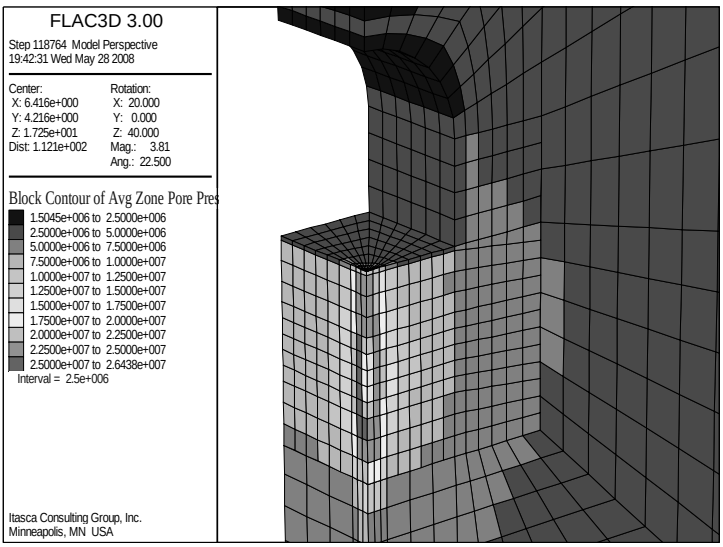

Fig. 53 Pore Water Pressure Contours for THM56.6K1.0

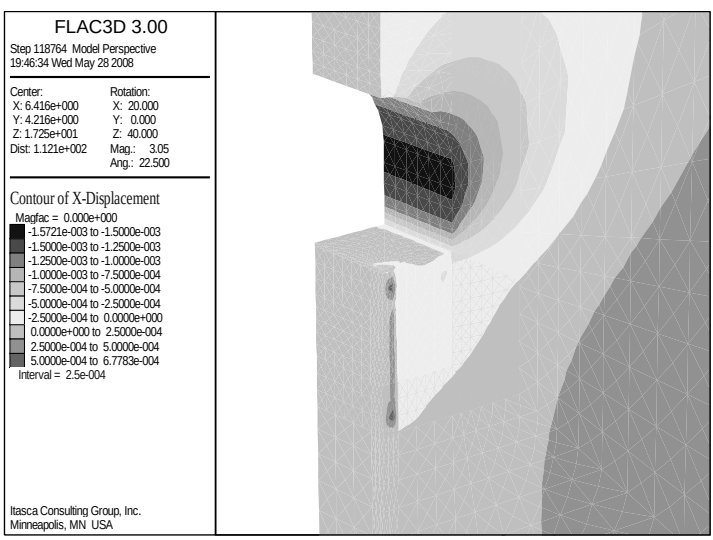

Fig. 54 X-Displacement Contours for THM56.6K1.0

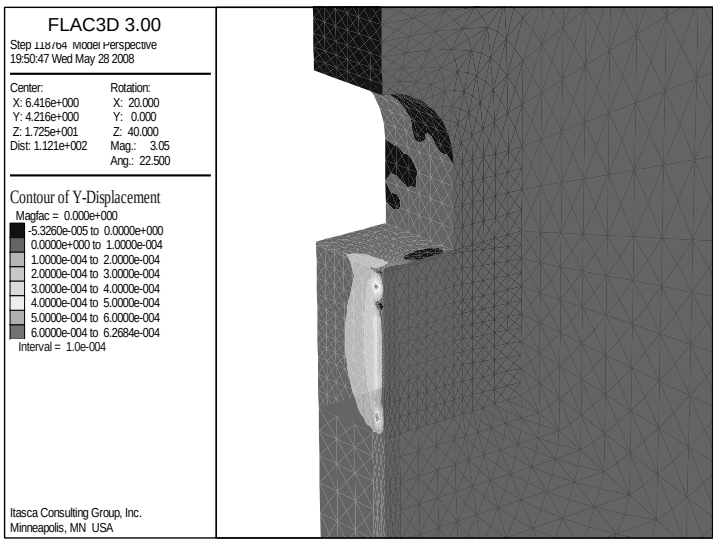

Fig. 55 Y-Displacement Contours for THM56.6K1.0

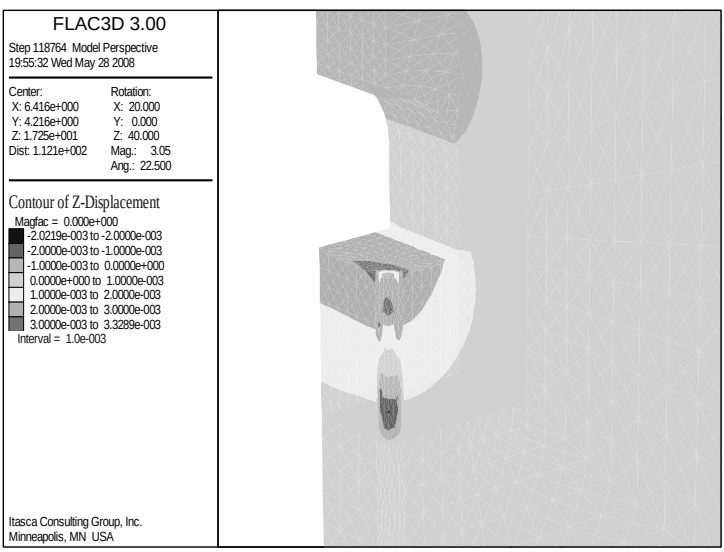

Fig. 56 Z-Displacement Contours for THM56.6K1.0

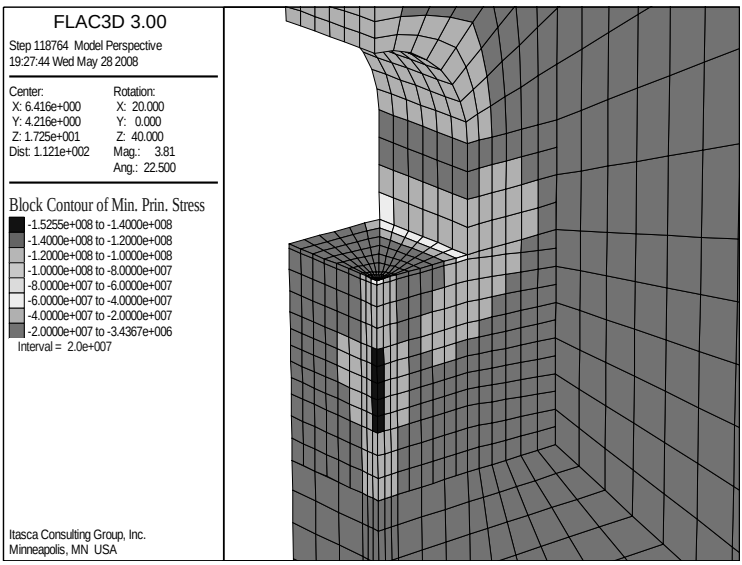

Fig. 57 Major Principal Stress Contours for THM56.6K1.0

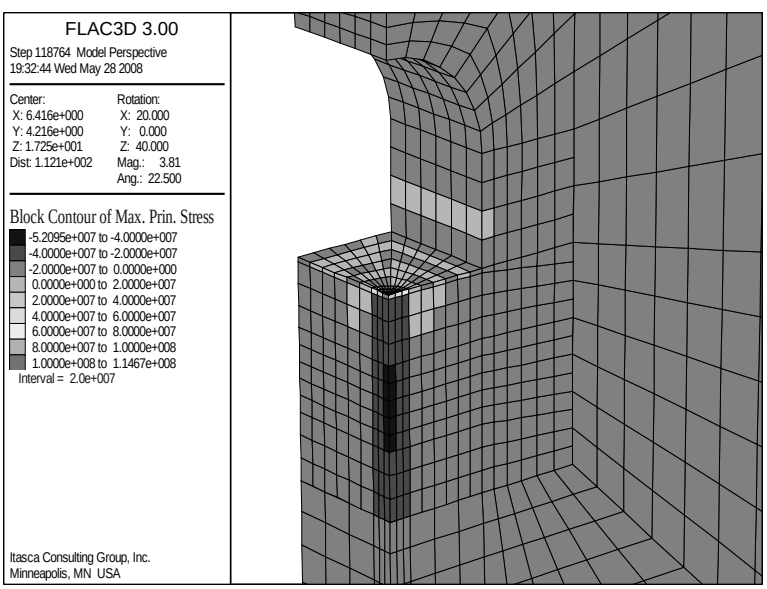

Fig. 58 Minor Principal Stress Contours for THM56.6K1.0

Table 15 Results of Thermo-Hydro-Mechanical Analysis THM56.6K1.0

Point	Principal stress*		X-displacement (mm)	Y-displacement (mm)	Z-displacement (mm)	Pore water pressure (MPa)
	Major (MPa)	Minor (MPa)				
1	-25.0	-1.725	0	0	-0.80	1.55
2	-18.7	-0.32	-1.550	0	0.75	3.15
3	-55.8	-11.3	-0.330	0	1.10	4.02
4	-4.2	+0.775	-0.095	0	3.075	5.15
5	-20.8	-10.0	-0.150	0	1.60	15.00
6	-17.9	-8.9	0.005	0	0.70	8.98
7	-152.5	-51.6	0	0	0.80	0.00
8	-28.2	-28.1	0	0.155	0.80	26.40
9	-21.2	-10.7	0	0.255	1.60	14.70
10	-18.5	-6.3	0	0	1.60	8.49
11	-147.6	-49.3	0	0	1.65	0.00
12	-10.6	+6.6	0	0.610	2.20	10.9
13	-50.4	-1.6	0	0	2.20	12.00
14	-25.0	-24.5	0	0	-1.20	19.00
15	-19.0	-13.9	0	0	0.60	12.00

* Compressive stress is negative.

Table 16 Comparison of Principal Stresses for Three Cases

Point	Major Principal Stress (MPa)			Minor Principal Stress (MPa)		
	M	TM	THM	M	TM	THM
1	-26.0	-25.8	-25.0	-1.8	-1.75	-1.725
2	-19.5	-16.5	-18.7	-9.2	-0.41	-0.32
3	-47.0	-47.5	-55.8	-0.8	-9.15	-11.3
4	-4.5	-5.14	-4.2	+1.0	+1.26	+0.775
5	-6.25	-6.62	-20.8	-3.0	-3.18	-10.0
6	-20.25	-15.0	-17.9	-7.0	-6.40	-8.9
7	-	-139.0	-152.5	-	-33.8	-51.6
8	-	-0.037	-28.2	-	+0.023	-28.1
9	-17.5	-16.5	-21.2	-3.0	-2.43	-10.7
10	-17.5	-17.1	-18.5	-5.55	-5.95	-6.3
11	-	-136.0	-147.6	-	-31.5	-49.3
12	-	-0.01	-10.6	-	-0.003	+6.6
13	-	-41.0	-50.4	-	-4.2	-1.6
14	-	-0.022	-25.0	-	-0.01	-24.5
15	-	-13.0	-19.0	-	-4.4	-13.9

* Compressive stress is negative.

Analysis of Circular Tunnel using Strain Softening Mohr-Coulomb Model

Many rocks in the field generally exhibit the phenomenon of strain softening under loads. The effect of strain softening is predominant around the tunnel boundary due to low confining pressure. Many models have been proposed to characterise strain softening behaviour. The models are presented in detail in Rakesh Kumar (2007). Sharma et al. (1985d) used Hoek-Brown strength criterion (Hoek and Brown, 1980) for the analysis of a circular tunnel with post-peak softening. In the following sections, strain softening Mohr-Coulomb model is presented and is used for the analysis of a circular tunnel.

Strain Softening Mohr-Coulomb Model

The strain softening Mohr-Coulomb model incorporated in FLAC software package has been used extensively for characterizing the post-peak softening behaviour of materials. In the conventional Mohr-Coulomb model (elastic-perfectly plastic), the strength parameters are assumed to remain constant. For the strain softening model, the difference lies in the possibility that the cohesion, friction, dilation and tensile strength may soften after the onset of plastic yield, although the yield and potential functions, plastic flow rules and stress corrections are identical to those of the conventional Mohr-Coulomb model. The user can define the cohesion, friction and dilation as piecewise-linear functions of the plastic shear strain. The details of the model are given in FLAC Version 4.0 manual (FLAC, 2002).

Analysis of a Circular Tunnel

Sandstone samples from Pancheswar Hydroelectric Project, Pancheshwar (Uttarakhand) were collected and strain controlled triaxial tests were conducted on the sandstone specimens at IIT Delhi (Rakesh Kumar, 2007). The stress-strain-volume change behaviour is shown in Figure 59.

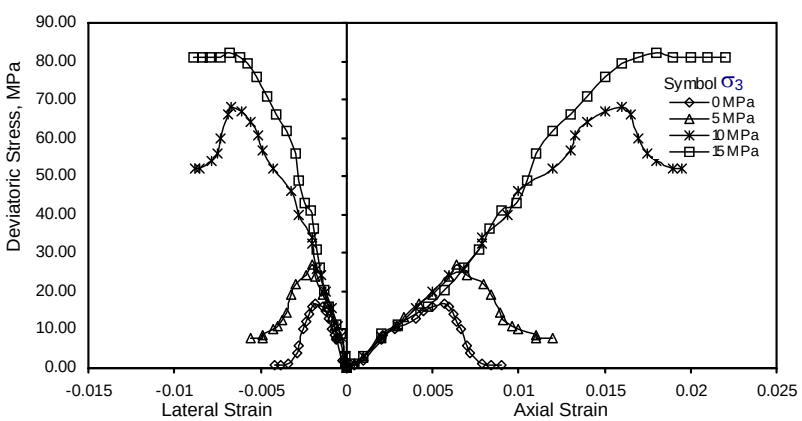

Fig. 59 (a)Stress-Strain-Volume Change Response of Pancheswar Sandstone - Stress-strain behaviour

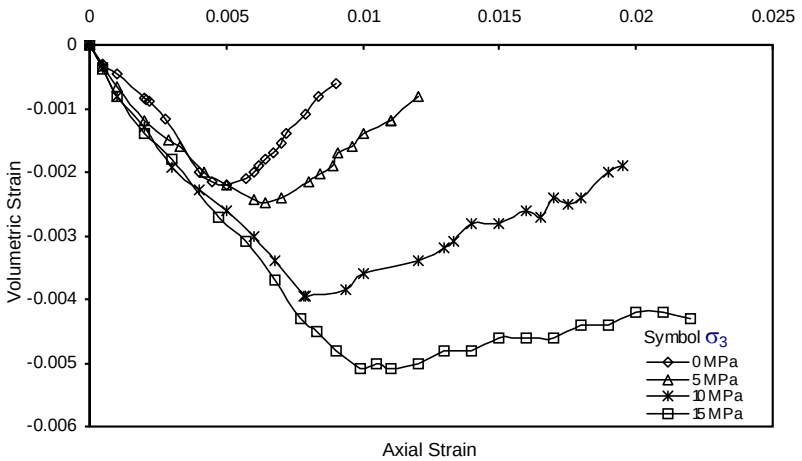

Fig. 59 (b) Stress-Strain-Volume Change Response of Pancheswar Sandstone - Volume change response

The characterization of the behaviour was done using strain softening Mohr-Coulomb model. The rock properties are given in Table 17.

Table 17 Properties of Pancheswar Sandstone

Properties	Value
Young's modulus, E	3940 MPa
Poisson's ratio, ν	0.30
Cohesion (peak)	2.29 MPa
Angle of friction (peak)	45.6°
Tensile strength	3.42 MPa
Dilation angle	18°
Density	22.2 kN/m^3

The post-peak variation of cohesion and friction angle with plastic shear strain, e^{ps} is shown in Figures 60 and 61, respectively. Using these properties, a circular tunnel of 10 m diameter, located at a depth of 500 m below ground surface, has been analysed (Rakesh Kumar, 2007; Rakesh Kumar et al., 2008). The rock has been assumed to be homogeneous and isotropic and the analysis has been carried out for three in-situ stress ratios of K_o = 0.5, 1.0 and 2.0. Two cases have been considered for the analysis:

(i) Case A: Conventional Mohr-Coulomb model using the peak values of cohesion, c = 2.29 MPa and friction angle, ϕ= 45.6° with K_o = 0.5, 1.0 and 2.0.

(ii) Case B: Mohr-Coulomb strain softening model with K_o = 0.5, 1.0 and 2.0 using post peak variation of cohesion and friction angle as per Figures 60 and 61.

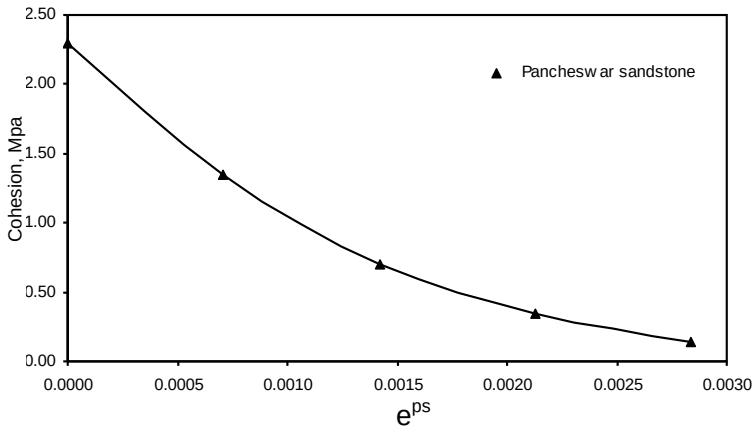

Fig. 60 Variation of Cohesion (c) with e^{ps} for Pancheswar Sandstone

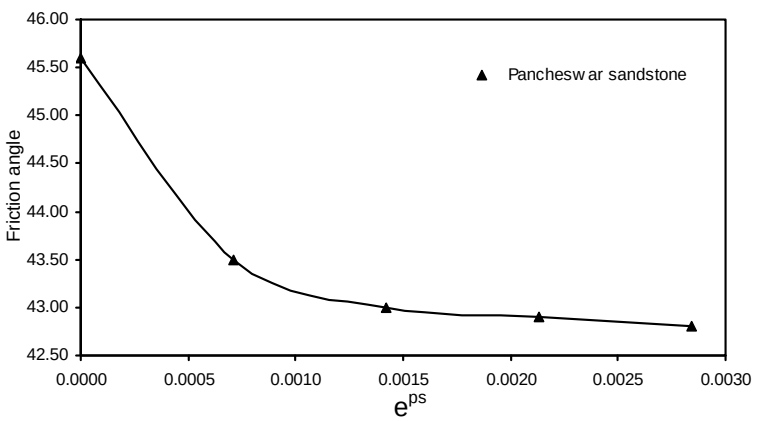

Fig. 61 Variation of Friction Angle (ϕ) with e^{ps} for Pancheswar Sandstone

Considering symmetry, only one quarter section of the tunnel is analysed assuming plane strain condition. An extent of five times the tunnel diameter is considered in both the directions to simulate infinity condition. A mesh of 625 four-noded quadrilateral elements is used for the analysis (Figure 62). The horizontal and vertical lines of symmetry are restrained in vertical and horizontal directions respectively. Uniform vertical pressure of σ_{vo} = 11.10 MPa corresponding to 500 m depth and uniform lateral pressure of $K_o \sigma_{vo}$ are applied on the outer horizontal and vertical boundaries respectively to simulate in-situ stress condition. The initial in-situ stress condition is applied to the model first and then the hole is removed in single step to simulate the tunnel excavation.

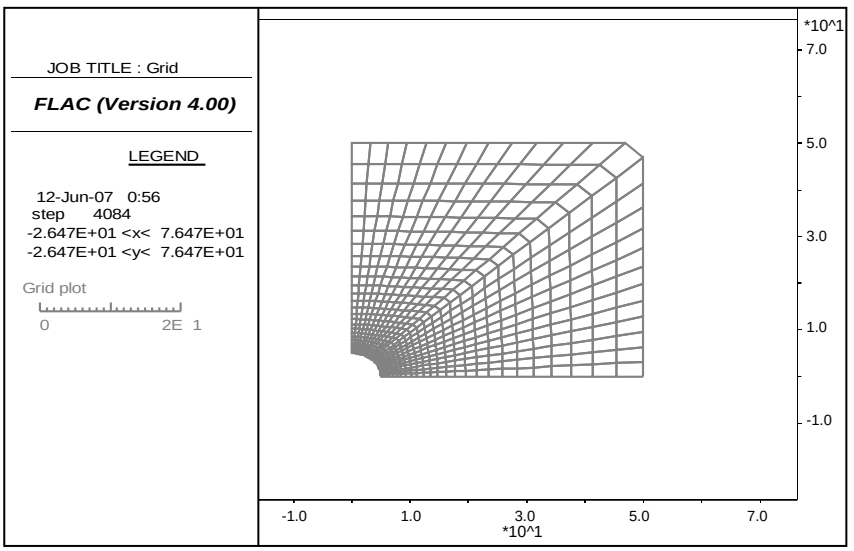

Fig. 62 Discretisation Scheme

The results of the analysis for the tunnel in terms of yielded zone, x-displacement, y-displacement, major and minor principal stress contours for three in-situ stress ratios for Case A and Case B have been described in detail by Rakesh Kumar (2007). The typical results for K_o = 0.5 in terms of yielded zone (Figures 63 and 64), and yielded zone, x-displacement, y-displacement, maximum and minimum principal stress values at crown and springing level of the tunnel (Table 18), have been presented below.

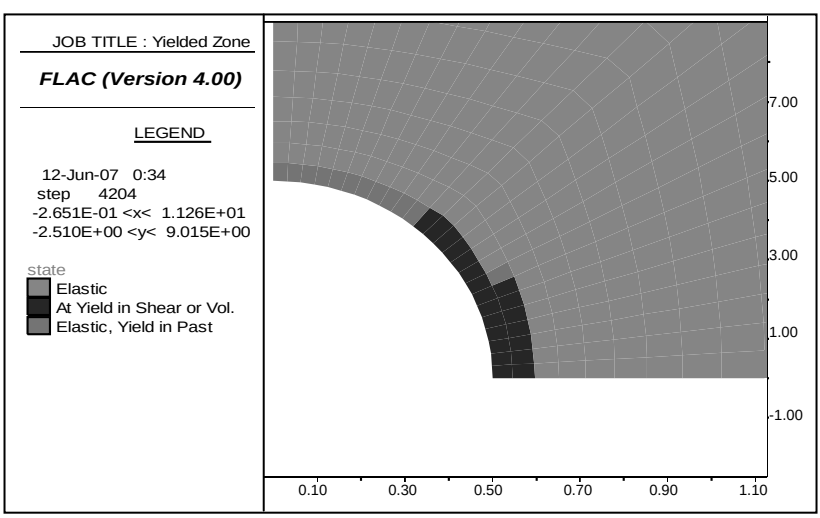

Fig. 63 Yielded Zone for the Tunnel Case A (K_o = 0.5)

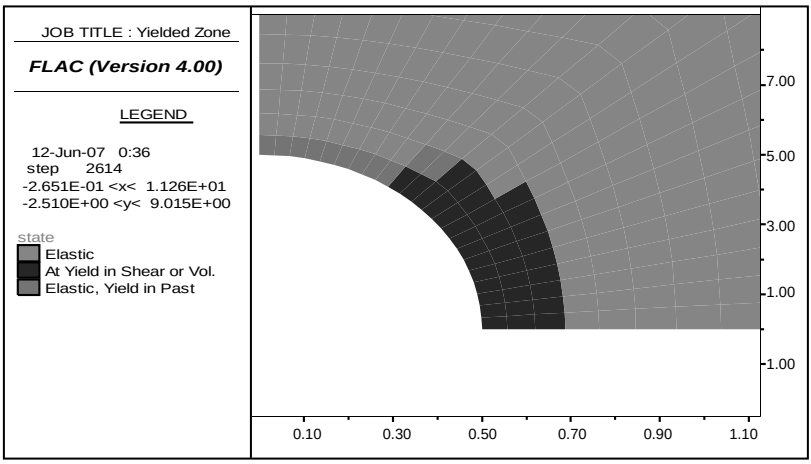

Fig. 64 Yielded Zone for the Tunnel Case B (K_o = 0.5)

Table 18 Comparison of Results for Mohr-Coulomb Model with and without Strain Softening for K_o = 0.5

Parameters	At crown			At springing level		
	Case A	Case B	Percentage Difference for Case B	Case A	Case B	Percentage Difference for Case B
Extent of Yielded Zone (m)	0.45	0.55	22 (Increase)	0.95	1.90	100 (Increase)
X-Displacement (mm)	0.00	0.00	0	9.94	44.13	344 (Increase)
Y-Displacement (mm)	24.47	29.78	22 (Increase)	0.00	0.00	0
Maximum Principal Stress (MPa)	5.76	4.59	20 (Decrease)	16.26	5.55	66 (Decrease)
Minimum Principal Stress (MPa)	0.34	0.28	18 (Decrease)	0.78	0.32	59 (Decrease)

As seen from Table 18 and Figures 63 and 64, for K_o = 0.5, the increase in the yielded zone is 22% at crown and 100% at springing level for Case B than that for Case A. The x-displacement at springing level is 344% more for Case B than that of Case A. The y-displacement at crown is 22% more for Case B than that of Case A. The maximum principal stress at springing level is 182% more for Case A and 21% more for Case B than that of crown. The decrease in the maximum principal stress is 20% at crown and 66% at springing level for Case B than that of Case A. The minimum principal stress at springing level is 129% more for Case A and 14% more for Case B than that of crown. The decrease in the minimum principal stress is 18% at crown and 59% at springing level for Case B than that of Case A. It is concluded that there is significant effect of strain softening on stress-deformation behaviour of tunnel, around and nearby the tunnel boundary. This is due to zero confinement to low confinement adjacent to the tunnel boundary.

Concluding Remarks

Underground structures are increasingly used in India for various purposes, the major use being for hydropower projects, mines and transportation and underground storage projects. For the design of these structures, conventional methods continue to be adopted. In recent times, various numerical methods, viz. finite element, boundary element and distinct element methods are increasingly used to study the behaviour of underground structures under two- and three-dimensional conditions. Constitutive models based on elastic, elasto-plastic and strain softening theories are used to characterize the behaviour of the intact rock and rock mass. The application of these methods to various problems has been presented in this paper and important conclusions are drawn. The predictions are compared with observed results in certain cases.

Acknowledgements

IIT Delhi provided the opportunity, impetus and encouragement to pursue the research work presented.

Most of the research work has been conducted in close collaboration with the author's former colleague Prof. A. Varadarajan. The research work presented in this paper has been primarily drawn from the work of the former research students, Dr. D.V. Thareja, Dr. R.B. Singh, Dr. R.K. Srivastava, Dr. M. Hashemi, Dr. H.R. Yadav and Dr. Rakesh Kumar, and former M.Tech. students Ms. Tanusree Chakroborty, Ms. Priyanka Jain, Ms. Archana, Mr. Aman Kumar, and Mr. S.K. Patel.

The research work on analysis of underground nuclear repository was partly supported by the Research Project on Thermo-hydro-mechanical Analysis of Underground Nuclear Repositories from Board of Research in Nuclear Sciences, Bhabha Atomic Research Centre, Government of India; and the research work on analysis of circular tunnel using strain softening Mohr-Coulomb model was partly supported by the Research Project on Testing and Constitutive Modelling of Rocks from Department of Science & Technology, Government of India.

The author expresses his sincere gratitude to his former colleagues Prof. T. Ramamurthy, Prof. S.K. Gulhati and Prof. G.V. Rao and colleagues Prof. Manoj Datta, Prof. K.S. Rao, Prof. J.M. Kate, Dr. G.V. Ramana Dr. K.K. Gupta, and Dr. J.T. Shahu for their help and encouragement and many fruitful discussions in connection with the research work presented in this paper.

References

ABAQUS (2004): *Theory and Users Manual, Online Version*, Hibbit, Karlsson and Sorensen Inc.

Aman Kumar (2005): *Finite Element Analysis of Underground AECL Type Nuclear Repository*, M. Tech. Thesis, submitted to the Department of Civil Engineering, IIT Delhi, India.

Archana (2007): *Rock Support Interaction Analysis in Underground Structures*, M. Tech. Thesis, submitted to the Department of Civil Engg., IIT Delhi, India.

Banerjee, P.K. and Butterfield, R. (1981): *Boundary Element Methods in Engineering Science*, McGraw-Hill.

Bathe, K.J. (1982): *Finite Element Procedures in Engineering Analysis*, Prentice-Hall, Inc., Englewood Cliffs, New Jersey.

Borja, R.I., Lee, S.R. and Seed, R.B. (1989): 'Numerical Simulation of Excavation in Elasto-Plastic Soils', *Int. J. Numer. Anal. Meth. Geomech.*, 13, pp. 231-249.

Brady, B.H.G.. (1987): 'Boundary Element and Linked Methods for Underground Excavation Design', Chapter 5 in *Analytical and Computational Methods in Engineering Rock Mechanics* (ed. E.T. Brown), Allen & Unwin, London, pp. 164-204.

Chakraborty, T. (2004): *Finite Element Analysis of Underground Nuclear Repositories*, M. Tech. Thesis, submitted to the Department of Civil Engineering, IIT Delhi, India.

Chakraborty, T. and Sharma, K.G. (2006): 'Finite Element Analysis of Underground Nuclear Repositories with Temperature Dependent Rock Properties', *Proc. 4th Asian Rock Mechanics Symposium*, Singapore, November.

Chandrasekaran, V.S. and King, G.J.W. (1974): 'Simulation of Excavation using Finite Elements', *J. Geotech. Engg. Div., ASCE*, 100, pp. 1086-1089.

Comodromos, E., Hatzigogos, Th. and Pitilakis, K. (1993): 'Multi-Stage Finite Element Algorithm for Excavation in Elasto-Plastic Soils', *Computers and Structures*, 46, pp. 289-298.

Crouch, S.L. and Starfield, A.M. (1983): *Boundary Element Method in Solid Mechanics,* George Allen & Unwin, London.

Cundall, P.A. (1971): 'A Computer Model for Simulating Progressive Large-Scale Movements in Blocky Rock Systems', *Proc. Symposium of the Int. Society for Rock Mechanics*, Nancy, Vol. 1, Paper No. II-8.

Desai, C.S. (1994): 'Hierarchical Single Surface and Disturbed State Constitutive Models with Emphasis on Geotechnical Application', Chap. 5 in *Geotechnical Engineering*, K.R. Saxena (Editor), Oxford & IBH Pub. Co., New Delhi, India.

Desai, C.S. (1997): *Manual for DSC-SST-2D: Computer Code for Static and Dynamic Solid, Structure and Soil-Structure Analysis*, Tucson, Arizona, U.S.A.

Desai, C.S. (2001): *Mechanics of Materials and Interfaces: The Disturbed State Concept*, Boca Raton FL, USA: CRC Press.

Desai, C.S. and Abel, J.F. (1972): *Introduction to the Finite Element Method,* Van Nostrand Reinhold Co., New York.

Desai, C.S., Sharma, K.G., Wathugala, G.W. and Rigby, D.B. (1991): 'Implementation of Hierarchical Single Surface $\delta 0$ and $\delta 1$ Models in Finite Element Procedure', Int. J. Numer. Anal. Meth. Geomech., 15, pp. 649-680.

DMRC (2002): *Geotechnical Interpretative Report*, Delhi Metro Rail Corp., India.

FLAC (2002): *Theory and Background Manual (version 4.0)*, Itasca Consulting Group Inc., Minneapolis, USA.

FLAC3D (2002): *Theory and Background Manual (version 4.0)*, Itasca Consulting Group Inc., Minneapolis, USA.

Ghaboussi, J. and Pecknold, D.A. (1984): 'Incremental Finite Element Analysis of Geometrically Altered Structures', *Int. J. Numerical. Methods in Engg*., 20, pp. 2051-2064.

Goodman, R.E. (1989): *Introduction to Rock Mechanics*, John Wiley & Sons.

Hashemi, M. (1999): *Constitutive Modelling of a Schistose Rock in the Himalaya*, Ph.D. Thesis submitted to Indian Institute of Technology Delhi, India.

Hoek, E. (1983): 'Strength of Jointed Rock Masses', Twenty-Third Rankine Lecture, *Geotechnique*, 33, pp. 185-222.

Hoek E and Brown ET. (1980): *Underground Excavations in Rock*, Institute of Mining and Metallurgy, London.

Jain, P. (2006): *Finite Element Analysis of Underground Nuclear Repositories,* M. Tech. Thesis, submitted to the Department of Civil Engg., IIT Delhi, India.

NIRM (1997): *Final Report: Rock Mechanics Instrumentation to Evaluate the Long-Term Stability of Powerhouse and Transformer Caverns at Nathpa-Jhakri Power Corporation (NJPC)*, National Institute of Rock Mechanics (NIRM), Kolar Gold Fields, Karnataka, India.

Obert, L. and Duvall, W.I. (1967): *Rock Mechanics and the Design of Structures in Rock*, John Wiley & Sons.

Patel, S.K. (2008): *Three-Dimensional Transient Thermo-Hydro-Mechanical Analysis of Underground Nuclear Repository*, M. Tech Thesis, submitted to the Department of Civil Engineering, IIT Delhi, India.

Patel, S.K. and Sharma, K.G. (2008): 'Three-Dimensional Transient Thermo-Hydro-Mechanical Analysis of Underground Nuclear Repository', *Proc. 5th Asian Rock Mechanics Symposium*, Tehran (Iran), November, Accepted.

Poulos, H.G. and Davis, E.H. (1974): *Elastic Solutions for Soil and Rock Mechanics*, John Wiley & Sons.

Pusch, R. (1994): *Waste Disposal in Rock*, Elsevier, Amsterdam.

Rakesh Kumar (2007): *Testing and Constitutive Modelling of the Strain-Softening Behaviour of Some Rocks*, Ph.D. Thesis submitted to Indian Institute of Technology Delhi, India.

Rakesh Kumar, Sharma, K.G. and Varadarajan, A. (2008): 'Effect of Strain-Softening on Tunnel Behaviour', *Proc. World Tunnelling Conference*, Agra (India), September, pp. 541-550.

Ramamurthy T. (1993): 'Strength and Modulus Responses of Anisotropic Rocks', Chap. 13 in *Comprehensive Rock Engineering*, Vol. I, Pergamon Press, Oxford, U.K., pp. 315-329.

Ramamurthy T. (2001): 'Shear Strength Response of Some Geological Materials in Triaxial Compression', *Int. J. Rock Mech. Min. Sci*., 38, pp. 683-697.

Rocscience (2006): *RocSupport, Version 3.007*, Rocscience Inc., Toronto.

Sharma, K.G. (2006): 'Thermo-Mechanical Analysis of Underground Nuclear Repositories using Finite Element Method', *Proc. 2nd Int. Conf. on Computational Mechanics and Simulations (ICCMS-06)*, Guwahati, December. Keynote Paper.

Sharma, K.G. (2007): *Thermo-Hydro-Mechanical Analysis of Underground Nuclear Repositories*, Research Project Report submitted to Board of Research in Nuclear Sciences, Bhabha Atomic Research Centre, Mumbai, India.

Sharma, K.G. and Pande, G.N. (1988): 'Stability of Rock Masses Reinforced by Passive, Fully-Grouted Rock Bolts', *Int. J. Rock Mech. Min. Sci. & Geomech. Abstr*., 25, pp. 273-285.

Sharma, K.G. and Pandya, A.B. (1988): 'Elasto-Plastic Finite Element Analysis of Tunnels in Reinforced Jointed Rock Mass', *Proc. Int. Symp. on Underground Engg*., New Delhi, April, pp. 199-206.

Sharma, K.G. and Sharma, M.K. (1986): 'Finite Element Analysis of Tunnels in Anisotropic Rock Medium', *Indian Geotechnical Journal*, 16(3), pp. 225-243.

Sharma, K.G., Varadarajan, A. and Desai, C.S. (2001): 'Improved Finite Element Simulation of Excavation in Elastic and Elasto-Plastic Geologic Media', *Journal of Rock Mechanics and Tunnelling Technology*, 7(1), pp. 11-28.

Sharma, K.G., Varadarajan, A. and Pandya, A.B. (1989): 'Circular Tunnel in Reinforced Jointed Rock Mass', *Proc. 3rd Int. Symp. on Numerical Models in Geomechanics*, Niagra Falls, Canada, May, pp. 524-535.

Sharma, K.G., Varadarajan, A. and Singh, R.B. (1985a): 'The Condensation of Boundary Element Stiffness Matrix in FEBEM Analysis', *Communications in Applied Numerical Methods*, 1, pp. 61-65.

Sharma, K.G., Varadarajan, A. and Srivastava, R.K. (1985b): 'Elasto-Viscoplastic Finite Element Analyses of Tunnels, *Proc. 5th Int. Conf. on Numerical Methods in Geomechanics*, Nagoya, April, 2, pp. 1141-1148.

Sharma, K.G., Varadarajan, A. and Srivastava, R.K. (1985c): Elasto-Plastic Finite Element Analysis of Interacting Tunnels', *Proc. Int. Conf. on Finite Elements in Computational Mechanics*, Bombay, December, pp. 301-310.

Sharma, K.G., Varadarajan, A. and Srivastava, R.K. (1985d): 'Elasto-Plastic Finite Element Analysis of a Circular Tunnel with Post Peak Softening', *Indian Geotechnical Journal*, 15(2), pp. 77-93.

Sharma, M.K. and Bagde, M.N. (1994): *Evaluation of Rock Properties and Analysis of Underground Cavern by FEM: Nathpa-Jhakri Project*, M.Tech. Thesis, submitted to the Department of Civil Engineering, IIT Delhi, India.

Singh, R.B. (1985): *Coupled FEBEM Analysis of Underground Openings*, Ph.D. Thesis submitted to Indian Institute of Technology Delhi, India.

Singh, R.B., Sharma, K.G. and Varadarajan, A. (1985): 'Elasto-Plastic Analysis of Circular Opening by FEBEM', *Proc. 2nd Int. Conf. on Computer Aided Analysis and Design in Civil Engineering*, Roorkee, January, III.128-III.134.

Singh, R.B., Sharma, K.G. and Varadarajan, A. (1988): 'Elasto-Plastic Analysis of Tunnel Excavation in Layered Rock Medium by Coupled FEBEM', *Proc. 6th Int. Conf. on Numerical Methods in Geomechanics*, Innsbruck, April, 2, pp. 941-950.

Singh, R.B., Sharma, K.G. and Varadarajan, A. (1989): 'Coupled Finite Element – Boundary Element Software for the Analysis of Underground Openings', *Proc. Int. Conf. on Engineering Software*, New Delhi, December, pp. 749-756.

Srivastava, R.K. (1985): *Elasto-Plastic Finite Element Analysis of Single and Interacting Tunnels*, Ph.D. Thesis submitted to Indian Institute of Technology Delhi, India.

Srivastava, R.K., Sharma, K.G. and Varadarajan, A. (1986a): 'Finite Element Analysis of Tunnels using Different Yield Criteria', *Proc. 2nd Int. Symp. on Numerical Models in Geomechanics*, Ghent, pp. 381-389.

Srivastava, R.K., Sharma, K.G. and Varadarajan, A. (1986b): 'Elasto-Plastic Finite Element Analysis of Circular Tunnels', *Indian Geotechnical Journal*, 16(4), pp. 295-316.

Srivastava, R.K., Sharma, K.G. and Varadarajan, A. (1987): 'Elasto-Plastic Finite Element Analysis of Horse-Shoe Tunnels', *Indian Geotechnical Journal*, 17(2), pp. 159-182.

Srivastava, R.K., Sharma, K.G. and Varadarajan, A. (1988): 'Analysis of Stresses in the Pillar Zone of Twin Circular Interacting Tunnels', *Proc. 6th Int. Conference. on Numerical Methods in Geomechanics*, Innsbruck, April, 3, pp. 1597-1606.

Srivastava, R.K., Sharma, K.G. and Varadarajan, A. (1989): 'Finite Element Analysis of Interacting Tunnels', *Proc. Indian Geotechnical Conference-89*, Vishakapatnam, December, pp. 325-330

TR (2004): *Technical Report*, Swedish Nuclear Fuel and Waste Management Co, Box 5864 SE-102 40, Stockholm, Sweden.

Terzaghi, K. and Richart, F.E. (1952): 'Stresses in Rock around Cavities', *Geotechnique*, 3(2), pp. 57-90.

Thareja, D.V. (1984): *Three-Dimensional Finite Element Analysis of Branching Tunnels*, Ph.D. Thesis submitted to Indian Institute of Technology Delhi, India.

Thareja, D.V., Sharma, K.G. and Madhavan, K. (1986): 'Finite Element Analysis of Steel Lined Branching Tunnels', *Proc. 2nd Int. Symp. on Numerical Models in Geomechanics*, Ghent, pp. 395-402.

Thareja, D.V., Sharma, K.G., Madhavan, K. and Natarajan, R. (1985): 'Three-Dimensional Finite Element Analysis of Branching Tunnels', *Proc. 5th Int. Conf. on Numerical Methods in Geomechanics*, Nagoya, April, 2, pp. 1193-1199.

Varadarajan, A. and Sharma, K.G. (1984a): *Finite Element Analysis of a Powerhouse Cavern in Gujarat*, Consultancy Report.

Varadarajan, A. and Sharma, K.G. (1984b): *Analysis of Powerhouse Cavern and Tunnel by Boundary Element Method*, Consultancy Report.

Varadarajan, A., Sharma, K.G., Desai, C.S. and Hashemi, M. (2001a): 'Constitutive Modelling of a Schistose Rock in the Himalaya', *International Journal of Geomechanics*, 1(1), pp. 83-107.

Varadarajan, A., Sharma, K.G., Desai, C.S. and Hashemi, M. (2001b): 'Analysis of a Powerhouse Cavern in the Himalaya', *International Journal of Geomechanics*, 1(1), pp.109-127.

Varadarajan, A., Sharma, K.G. and Singh, R.B.. (1983a): 'Analysis of Tunnels by Boundary Element Method', *Indian Geotechnical Journal*, 13(4), pp. 249-268.

Varadarajan, A., Sharma, K.G. and Singh, R.B. (1983b): 'Analysis of Circular Tunnel by Coupled FEBEM', *Proc. Indian Geotechnical Conference-83*, Madras, pp. 113-118.

Varadarajan, A., Sharma, K.G. and Singh, R.B. (1985a): 'Analysis of Underground Openings by FEBEM', *Proc. 5th Int. Conf. on Numerical Methods in Geomechanics*, Nagoya, April, 2, pp. 1063-1069.

Varadarajan, A., Sharma, K.G. and Singh, R.B. (1985b): 'Some Aspects of Coupled FEBEM Analysis of Underground Openings', *Int. J. Numer. Anal. Meth. Geomech.*, 9, pp. 557-571.

Varadarajan, A., Sharma, K.G. and Singh, R.B. (1987): 'Elasto-Plastic Analysis of an Underground Opening by FEM and Coupled FEBEM', *Int. J. Numer. Anal. Meth. Geomech.*, 11, pp. 475-487.

Yadav, H.R. (2005): *Geotechnical Evaluation and Analysis of Delhi Metro Tunnels*, Ph.D. Thesis submitted to Indian Institute of Technology Delhi, India.

Zienkiewicz, O.C. and Pande, G.N. (1977): 'Time Dependent Multi-Laminate Model of Rocks- A Numerical Study of Deformation and Failure of Rock Masses', *Int. J. Numer. Anal. Meth. Geomech.*, 1, pp. 219-247.

Zienkiewicz, O.C. and Taylor, R.L. (1989): *The Finite Element Method*, International Edition, McGraw-Hill, Singapore.